

Emerging Structure–Function Relations in the Developing Face Processing System

K. Suzanne Scherf¹, Cibu Thomas^{2,3}, Jaime Doyle⁴ and Marlene Behrmann^{4,5}

¹Department of Psychology, The Pennsylvania State University, University Park, PA, USA, ²Laboratory of Brain and Cognition, National Institute of Mental Health, National Institutes of Health, Bethesda, MD 20892, USA, ³Center for Neuroscience and Regenerative Medicine at the Uniformed Services, University of the Health Sciences, Bethesda, MD 20892, USA, ⁴Department of Psychology, Carnegie Mellon University, Pittsburgh, PA 15213, USA and ⁵Center for the Neural Basis of Cognition, Pittsburgh, PA 15213, USA

Address correspondence to K. Suzanne Scherf, Department of Psychology, 111 Moore Hall, The Pennsylvania State University, University Park, PA 16802, USA. Email: suzyscherf@psu.edu

To evaluate emerging structure–function relations in a neural circuit that mediates complex behavior, we investigated age-related differences among cortical regions that support face recognition behavior and the fiber tracts through which they transmit and receive signals using functional neuroimaging and diffusion tensor imaging. In a large sample of human participants (aged 6–23 years), we derived the microstructural and volumetric properties of the inferior longitudinal fasciculus (ILF), the inferior fronto-occipital fasciculus, and control tracts, using independently defined anatomical markers. We also determined the functional characteristics of core face- and place-selective regions that are distributed along the trajectory of the pathways of interest. We observed disproportionately large age-related differences in the volume, fractional anisotropy, and mean and radial, but not axial, diffusivities of the ILF. Critically, these differences in the structural properties of the ILF were tightly and specifically linked with an age-related increase in the size of a key face-selective functional region, the fusiform face area. This dynamic association between emerging structural and functional architecture in the developing brain may provide important clues about the mechanisms by which neural circuits become organized and optimized in the human cortex.

Keywords: adolescent, child, development, DTI, fMRI, IFOF, ILF, visual processing

Introduction

The neural architecture supporting cognition is increasingly being conceptualized as a complex distributed system (e.g., McIntosh 2004; Catani 2007). In other words, functional specialization is not simply an intrinsic property of individual regions that compute specific representations and/or computations in isolation, but rather is an emergent property of the interactions between a set of spatially distributed nodes and their functional and structural connections to one another (e.g., Haxby et al. 2000; Gobbini and Haxby 2007; Vuilleumier and Pourtois 2007). Consequently, there is an emerging emphasis on characterizing the properties of broad, spatially distributed networks, including the functional and structural properties of both the nodes and the connections between these nodes. The goal of the current investigation was to begin to understand the developmental emergence of these network characteristics and we do so using the integrated circuit mediating face perception as the model domain. Given that the face/object processing network has been identified as a core functional brain network (Mesulam 1990), studying its development provides a unique opportunity to uncover its emerging dynamics and to elucidate the development of complex distributed circuits, more generally.

There is growing consensus that mature face recognition is mediated by a distributed neural circuit (Haxby et al. 2000; Fairhall and Ishai 2007; Gobbini and Haxby 2007; Vuilleumier and Pourtois 2007; Ishai 2008), which includes a set of “core” and “extended” nodes or regions (Haxby et al. 2000, 2002; Gobbini and Haxby 2007). The core regions include the “occipital face area” (OFA; Gauthier et al. 2000), the “fusiform face area” (FFA; Kanwisher et al. 1997), and the posterior superior temporal sulcus (Hoffman and Haxby 2000). These core regions send and receive inputs to/from the extended regions, including the amygdala, insula, and medial prefrontal cortex, regions in the anterior paracingulate cortex, and the anterior temporal pole (Gobbini and Haxby 2007). An emerging perspective argues that functional specialization within this distributed network emerges from modulations in the “interactions among the nodes” to produce the seemingly localized computations of face processing that have been previously ascribed to individual regions (Nestor et al. 2011). Building from this perspective, the central question addressed here concerns how this complex distributed network emerges and becomes functionally integrated over the course of development.

Developmental studies investigating the neural basis of face processing have primarily focused on age-related differences in the functional properties of the posterior core regions (Pasarotti et al. 2003, 2007; Gathers et al. 2004; Aylward et al. 2005; Golarai et al. 2007, 2010; Peelen et al. 2009; Joseph et al. 2011). For example, we have shown that, unlike adults, young children (aged 5–8 years) do not exhibit consistent group-level face-related activation in either hemisphere (Scherf et al. 2007). When these regions are identified within individual participants, there is a linear relation between the size/volume of the face-processing regions and age (Golarai et al. 2007, 2010; Scherf et al. 2007, 2011). Interestingly, in contrast to the volume, the magnitude of selectivity within these regions appears to be more adult-like earlier in development (Pelphrey et al. 2009; Cantlon et al. 2011), particularly when the regions are identified in each participant individually (Scherf et al. 2007, 2011). Importantly, the representational capacity of these regions to encode individual faces continues to change into young adulthood, even when their topographic organization has become adult-like in adolescence (Scherf et al. 2011). There is also evidence to suggest that the functional interactions between these nodes change with age as well (Cohen Kadosh et al. 2011), which could result from continued developmental specialization within each of these regions. However, the protracted emergence of the interaction between the individual nodes of the circuitry supporting face perception might also be contingent on the development of the “structural connections” between the nodes.

Here, we examine age-related differences in the structural properties of the fiber tracts connecting the multifocal nodes of the neural circuitry supporting face perception. In addition, we evaluate whether the emergence of efficient functional organization within this network is related to such structural differences. The process of myelination alters the architecture of white matter tracts and, in so doing, facilitates faster transmission of neural signals. Myelination of both short- and long-range fiber tracts continues into early adulthood (Benes et al. 1994; Lebel and Beaulieu 2011), leading to the hypothesis that the slow process of myelination may be particularly rate limiting with respect to the development of efficient long-range functional circuits. In addition, given the evidence of activity dependent influences on the processes of myelination in adults (for review, see Thomas and Baker 2012), developmentally emerging structure–function relations in the face-processing network might be mediated by increases in regionally specific neural activation. This activation may, in turn, induce changes in diffusion parameters of the connecting fiber tracts, thus enabling more specific and efficient network functioning.

The inferior longitudinal fasciculus (ILF) and the inferior fronto-occipital fasciculus (IFOF) are 2 major white matter fiber tracts that propagate signals to the ventral visual cortex, the anterior temporal lobe, and the frontal cortex, respectively. The ILF is the primary occipito-temporal associative tract (Crosby et al. 1962; Gloor 1997). Recent methodological advances in diffusion tensor imaging (DTI) and fiber tractography have demonstrated that (1) the course and termination of a major associative connection between the occipital and anterior temporal lobes are consistent with classical anatomical descriptions of the ILF in humans and with the monkey visual anatomy (Schmahmann et al. 2007); and (2) the tractography-defined ILF is structurally distinct from fibers of the optic radiation and from U-shaped fibers connecting adjacent gyri (Catani et al. 2003). The IFOF begins in the occipital cortex, continues medially through the temporal cortex dorsal to the uncinate fasciculus, and terminates in the inferior frontal and dorsolateral frontal cortex (Catani et al. 2002). Recently, functional neuroimaging and magnetoencephalography studies have provided supporting, albeit indirect, evidence of rapid interactions between posterior ventral visual areas and more anterior regions (e.g., anterior temporal lobe and amygdala) that implicate the involvement of long-range association fiber tracts that connect these regions, including the ILF and the IFOF (Bar et al. 2006; Rudrauf et al. 2008; Gschwind et al. 2012). Finally, damage to either pathway disrupts face processing (Catani et al. 2003; Catani and Thiebaut de Schotten 2008; Fox et al. 2008; Philippi et al. 2009; Thomas et al. 2009), suggesting that these white matter tracts are a critical component of the neural system necessary for face processing.

Prevailing evidence also suggests that both the ILF and the IFOF undergo age-related increases in their structural properties from early childhood to adulthood (Lebel et al. 2008; Loenneker et al. 2011), suggesting that intrahemispheric connectivity increases within these tracts. Importantly, impressive age-related increases in the volume (a macrostructural index of the tract architecture) of the ILF and IFOF were reported in a longitudinal sample of healthy individuals ages 5–32 years who were scanned at least twice with a mean gap between scans of 4 years (Lebel and Beaulieu 2011). Of particular relevance for the current investigation, the ILF was 1 of 3 tracts

that exhibited prolonged age-related changes such that 40–53% of the oldest participants showed volume increases across the 2 scanning sessions. In a cross-sectional sample of these same participants, the ILF did not plateau with respect to the development of its microstructural properties (i.e., mean diffusivity, MD) until the age of 18, whereas the IFOF plateaued earlier at the age of 14 (Lebel et al. 2008).

As evident, several studies have explored age-related changes either in functional or in structural architectural changes across development. A very few developmental neuroimaging studies have examined both structural and functional changes and their interactions, and none has done so specifically in the context of face perception. Here, we examine whether developmental differences in the structural integrity of the ILF and IFOF, defined independently using anatomical regions of interest (ROIs), are related to developmental differences in the characteristics of the functional regions connected by these tracts. We evaluated differences across participants whose ages covered a substantial range (ages 6–23 years) in (1) the macro- and microstructural properties of the fasciculi that connect core and extended regions of the face-processing network using DTI, and in (2) the functional profile (size, location, and magnitude of selectivity) of the individual regions using functional magnetic resonance imaging (fMRI). We predicted a positive association between the structural and functional properties of the emerging face-processing circuit that would increase with age. Specifically, we expected that age-related differences in both the macro- (e.g., volume) and micro- [e.g., fractional anisotropy (FA), MD, radial diffusivity (RD)] structural properties of the ILF and IFOF, particularly in the right hemisphere, would be associated with the functional characteristics of the FFA and OFA. To determine the specificity of the differences, we also characterized 2 control tracts (forceps major, F-Ma and forceps minor, F-Mi), and a control functional region (the parahippocampal place area, PPA) in which developmental differences might also be evident, but whose profile should be unrelated to the changes in face-selective blood oxygen level-dependent (BOLD) activation.

Materials and Methods

Participants

Participants included 50 healthy individuals (age: 6–23 years; $M = 15.6$, $SD = 5.8$; 38 males). A subset of 35 of these individuals (age: 6–23 years; $M = 14.6$, $SD = 5.9$; 26 males) also participated in a functional neuroimaging study in the same scanning session to localize face and place processing ROIs. The distribution of participants across the age range was similar in the full sample as well as in the smaller sample of participants who also participated in the fMRI study, including approximately 14% (DTI = 7 and fMRI = 5) in the 6–8 year range, 23% (DTI = 9 and fMRI = 8) in the 9–11 year range, 26% (DTI = 10 and fMRI = 9) in the 12–14 year range, 6% (DTI = 5 and fMRI = 1) in the 15–20 year range, and 34% (DTI = 19 and fMRI = 12) in the 21–23 year age range.

Neither the participants nor their first-degree relatives had any history of neurological or psychiatric disorders, as determined in an interview with participants or participants' parents. All were right-handed and had normal or corrected vision. Participants and/or their guardian provided informed consent prior to participating in the study. All the experimental procedures were approved by the University of Pittsburgh and Carnegie Mellon University Internal Review Boards.

Stimuli and Procedure

Immediately prior to the scanning session, all participants were trained extensively in a mock scanner for 15–30 min. Each participant (including all adults) practiced lying still while watching a movie inside the

mock scanner with the simulated noise. During this mock session, participants were instructed on how to engage in relaxation breathing, given mental imagery upon which to focus (e.g., lying in own bed watching a movie), and provided with feedback about when they moved during the simulation. This extensive simulation procedure reduces anxiety and motion during the full scan, particularly in young children, but also in adults.

Participants were scanned at the Brain Imaging Research Center in Pittsburgh on a Siemens 3-T Allegra Scanner (Erlangen, Germany). During the scanning session, the stimuli were displayed on a rear-projection screen located inside the MR scanner. A movie localizer task (Hasson et al. 2004) was used to map face- and place-sensitive regions in individual participants. The movie localizer included a silent, fluid concatenation of short (15-s) movie vignettes (32 in total), containing either scenes of people and faces, buildings, navigation through open fields, or miscellaneous common objects (i.e., 4 experimental conditions) that lasted approximately 9 min. This passive viewing task, employing rich visual inputs, has been used successfully to map face- and place-selective activation in individual children as young as 5 years of age (face- and place selectivity can be identified in approximately 85% of individual children: Scherf et al. 2007). Functional data from a subset of the participants have been reported previously (Scherf et al. 2007, 2010).

MRI Scanning

MRI images were acquired on the scanner equipped with a standard quadrature birdcage head coil. Diffusion-weighted data were acquired based on a single-shot echo, echo-planar imaging (EPI) sequence with diffusion sensitizing gradients applied on either side of the 180° refocusing pulse. Diffusion-weighted images of the whole brain were acquired along the horizontal plane along 6 noncollinear directions. A reference image with no diffusion weighting ($b = 0$) was also obtained. The DTI scan lasted a total of 7 min and included the following parameters: time repetition (TR) = 4900 ms, time echo (TE) = 82 ms, flip angle = 90°, 210 × 210 mm² field of view, 80 × 128 acquisition matrix, 34 axial slices, 3 mm slice thickness, 1.64 × 1.64 mm² pixels, diffusion weighting $b = 850$ s/mm². Twelve repetitions of the complete set were collected and averaged to increase the signal-to-noise ratio without introducing motion artifacts. High-resolution anatomical images were also acquired during the same scanning session for each participant using a 3-dimensional (3D) magnetization-prepared rapid gradient echo pulse sequence with 192 1-mm T_1 -weighted, straight sagittal slices. For the functional localizer paradigm, EPI BOLD images were acquired in 35 anterior commissure - posterior commissure aligned slices and covered most of the brain and all of the occipital and temporal lobes (TR = 3000 ms; TE = 35 ms; 64 × 64, 3 mm slice thickness, 3.203 × 3.203 mm in-plane resolution).

Image Processing and Data Analyses

Diffusion-Weighted Data

The diffusion-weighted data processing and fiber tracking were performed in the native space of each subject using DTIStudio (Jiang et al. 2006), which calculates diffusion tensors by using least square fitting. By diagonalizing the diffusion tensor for each voxel, the program generates as output the 6 components of a diffusion tensor (D_{xx}, D_{yy}, D_{zz}, D_{xy}, D_{xz}, and D_{yz}), 3 eigenvectors that characterize the direction of diffusion, and 3 eigenvalues that characterize the magnitude of the diffusion in the corresponding eigenvector. A tensor-smoothing algorithm (Westin et al. 2002) was employed to reduce residual errors (Jones et al. 2005), particularly in the long-range fiber tracts that can prematurely terminate due to increasing noise as fiber length increases (Lori et al. 2002). From the diffusion tensor, FA, and diffusivity values were generated for each pixel, including MD, axial diffusivity (AD), and radial diffusivity (RD) in 10⁻³ mm²/s. MD is computed as the

average of the 3 eigenvalues, AD (i.e., parallel diffusivity) reflects the diffusivity along the principal axis (λ_1), and RD (i.e., perpendicular diffusivity) is defined as the average of the second and third eigenvalues [$\lambda_{\perp} = (\lambda_2 + \lambda_3)/2$] and has been shown by several researchers to be a marker of myelination (Beaulieu 2002; Song et al. 2005).

Determination of the White Matter Tracts of Interest

For fiber tracking, DTIStudio uses 3 parameters to generate 3D fiber tracts based on the Fiber Assignment of Continuous Tracking (FACT) algorithm and a brute-force fiber reconstruction approach (Mori et al. 1999; Xue et al. 1999). These parameters were specified as follows: The minimum FA threshold to initiate and terminate tracking was set to 0.20, which is typically appropriate for segmenting gray from white matter (Cercignani et al. 2001), and the critical angle threshold to terminate tracking in the event of a sharp turn in fiber direction was set to 40°. Within each tract, the volume (the number of voxels through which the fibers pass multiplied by the volume of the voxel) as well as the mean FA, MD, AD, and RD values across these voxels were extracted. If the streamlines of a particular fasciculus were not extracted in a particular participant, a score of 0 was entered for the volume of the fasciculus and the mean FA, MD, RD, and AD values (as determined by the entire sample) for the particular fasciculus were used so that each participant could contribute to each regression analysis of tract measures and age. We also ran secondary analyses excluding these participants from the analyses to evaluate whether the pattern of results differed in any way.

To extract the tracts of interest, we used a multiple ROI approach developed in a previously defined protocol (Thomas et al. 2008, 2009) that was very similar in procedure to that used by Wakana et al. (2007) for identifying the ILF, IFOF, F-Ma, and F-Mi. This approach is less susceptible to noise and partial volume effects, particularly when used in conjunction with brute-force fiber reconstruction. To delineate these ROIs accurately, we coregistered and resliced the high-resolution T_1 -weighted images with the $b = 0$ images of the diffusion-weighted images using SPM2 (Wellcome Department of Cognitive Neurology, London, UK) and an in-house Matlab program. The coregistered dicom images were imported to the DTI studio image viewer so that the user-defined ROIs could be demarcated. We defined ROIs using anatomical markers along the mid-sagittal plane in the native space for each individual (Fig. 1). Briefly, a source ROI (ROI-1) and a target ROI (ROI-2) were identified for each tract in each participant separately. To ensure maximum recovery of fibers within each fasciculus, fibers were only extracted if they passed through both ROIs in both directions (ROI-1 to ROI-2 as well as ROI-2 to ROI-1) and were not included in another tract. This DTI and tractography protocol has been used successfully to evaluate developmental declines in ILF and IFOF properties in aging individuals (Thomas et al. 2008), as well as group differences in properties of these tracts in individuals with developmental disorders (Thomas et al. 2009, 2011).

Inferior fronto-occipital fasciculus. For each hemisphere, ROI-1 was defined as the ventral aspect of the occipito-temporal cortex (VOTC) inferior to the floor of the posterior horn of the lateral ventricles on the first coronal slice posterior to the splenium of the corpus callosum (see Fig. 1a–b). Because the IFOF shares a similar fiber trajectory with the ILF until the floor

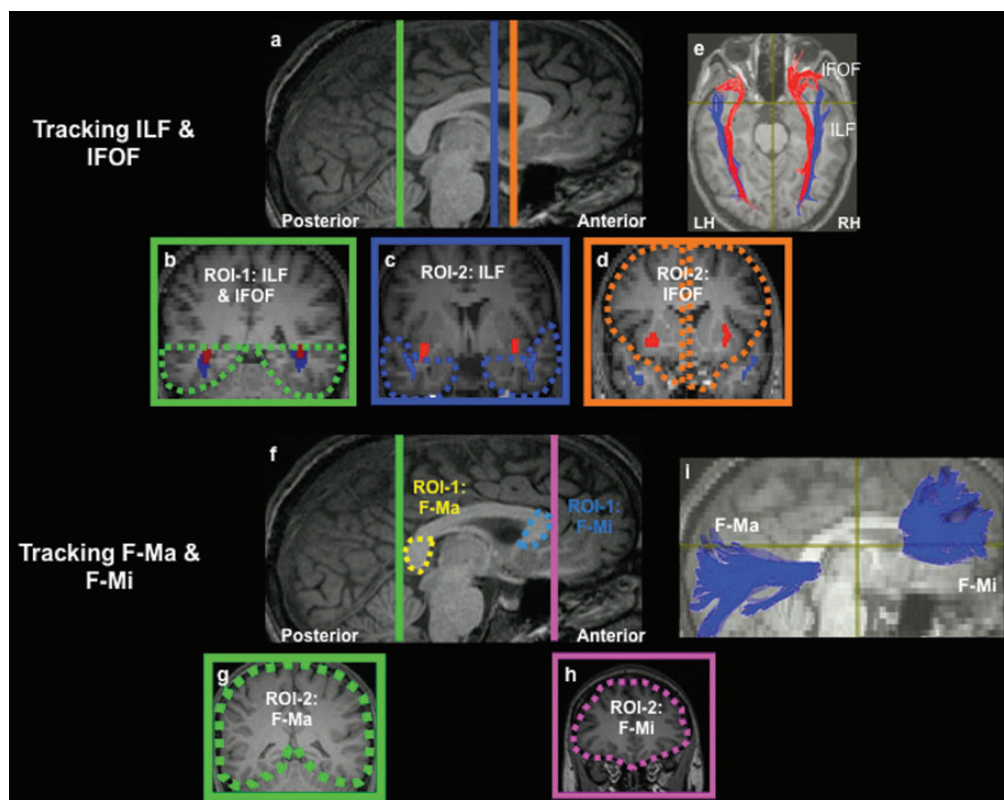


Figure 1. ROIs for DTI tractography. Illustration of the protocol used for extracting the tracts of interest. (a) Mid-sagittal slice shows the relative locations of the coronal slices on which the ILF and IFOF ROIs were defined in native space. Clockwise from (b) to (d), the coronal slices are color coordinated to indicate their corresponding position on the mid-sagittal plane. To extract the ILF, the VOTC inferior to the lateral ventricles was defined as ROI-1 (b) and the entire temporal cortex anterior to the point where the fornix descends to the mammillary bodies was defined as ROI-2 (c). To extract the IFOF, ROI-1 was the same as the one used for the ILF (b), but the entire frontal cortex anterior to the rostrum of the callosum was defined as ROI-2 (d). Note that each tract was extracted by including streamlines that project through the 2 ROIs and by excluding tracts that belong to other fiber systems. (e) The ILF (blue) and IFOF (red) are extracted and displayed on the mid-sagittal plane on a single diffusion-weighted slice coregistered onto the corresponding T_1 high-resolution slice. To extract the F-Ma and F-Mi, the splenium and genu of the corpus callosum were delineated on the mid-sagittal slice (f). For the F-Ma: the splenium (f) was defined as ROI-1 and the first coronal slice posterior to the splenium of the corpus callosum (g) was defined as ROI-2. For the F-Mi: the genu and rostrum (f) of the callosum were defined as ROI-1 and the first coronal slice anterior to the genu (h) was defined as ROI-2. (i) The approximate trajectory of the callosal tracts. All images displayed are in neurological convention.

of the external capsule, to avoid inclusion of the ILF fibers, ROI-2 was defined as the region of the frontal cortex on the first coronal slice posterior to the tip of the rostrum of the corpus callosum in each hemisphere (see Fig. 1d). Thus, the IFOF was defined as the set of long-range fibers between the posterior VOTC region and the entire frontal cortex of each hemisphere. After the IFOF fibers were extracted, they were removed from the analysis using the NOT operation to prevent inclusion of the fibers during extraction of the ILF fibers.

Inferior longitudinal fasciculus. ROI-1 was the same for extraction of ILF and IFOF fibers (see Fig. 1a–b). To avoid including the optic radiation from the lateral geniculate nucleus of the thalamus, and considering the fact that the ILF extends to the anterior temporal cortex with lateral and medial branches, ROI-2 was defined as the anterior region of the temporal cortex on the coronal slice coinciding with the point where the fornix descends toward the mammillary bodies (see Fig. 1c). Thus, for each hemisphere, the ILF was defined as the set of long-range fibers between the VOTC anterior temporal cortex.

Forceps major. ROI-1 was defined as the entire coronal slice posterior to the caudal tip of the splenium of the corpus callosum, observable on the mid-sagittal plane (see Fig. 1f).

ROI-2 was defined as the splenium of the callosum (see Fig. 1g). Because there is substantial individual variability in the morphology of the corpus callosum, the splenium was delineated on the mid-sagittal plane as the bulbous portion of the callosum that was inferior to the posterior aspect of the callosum. The splenium is also known to be the path for a group of fibers known as the tapetum, which project bilaterally through the walls of the lateral ventricles. Because these fibers were not the focus of this investigation, the fibers belonging to the tapetum were removed using the NOT operation before quantifying the integrity of the fibers. Thus, the F-Ma encompassed the fibers from the parietal, dorsal-occipital, and ventral-occipital regions that projected only through the splenium of the callosum.

Forceps minor. On the mid-sagittal plane, the first coronal slice anterior to the genu of the callosum, which encompassed the entire frontal cortex anterior to the corpus callosum in both hemispheres, was defined as ROI-1 (see Fig. 1f). The rostrum and genu of the corpus callosum were defined on the mid-sagittal plane as ROI-2 (see Fig. 1h). As before, to control for individual variability in the morphology of the callosum, ROI-2 was defined on the mid-sagittal plane by placing the coronal slice marker along the most posterior tip of the

rostrum and by delineating the region of the callosum anterior to the rostrum and body of the callosum. Thus, the F-Mi fibers included the fibers from the superior and inferior fronto-polar gyrus and fronto-marginal gyrus passing through the genu and the rostrum of the callosum.

fMRI Data

The data were analyzed using Brain Voyager QX (Brain Innovation, Maastricht, Netherlands). Preprocessing of functional images included 3D-motion correction, filtering out of low frequencies, and resampling the voxels to 1 mm^3 . The functional data were not spatially smoothed. Only participants who exhibited maximum motion of <1 voxel (3 mm) in all 6 directions (i. e., no spikes in motion $>2.9\text{ mm}$ in any direction on any image) were included in the fMRI analyses and fMRI-DTI correlation analyses. This is standard practice in both developmental and adult neuroimaging studies (Wilke et al. 2005; Nemani et al. 2009). In addition, we also evaluated whether mean motion in each of the 6 directions was correlated with age. Mean motion did not exceed half a voxel (1.5 mm) in any individual in any direction. However, separate linear regressions of age on motion estimates in each direction revealed that age was weakly correlated with motion in 2 directions, that is, translation along the y -axis, $F_{1, 35} = 4.9$, $P < 0.05$, and translation along the z -axis, $F_{1, 35} = 4.3$, $P = 0.05$. To ensure that any findings of age-related differences in the fMRI analyses and fMRI-DTI correlations were not simply due to motion, we included the mean motion for each of these directions as covariates in regression analyses.

To analyze the BOLD data generated from the fMRI scan, the time-series images for each brain volume in each participant were analyzed for stimulus category and/or experimental condition differences in a fixed-factor general linear model (GLM). The GLM was computed on the z -normalized raw signal in each voxel. Each of the categories/conditions was defined as a separate predictor and was modeled with a box-car function, which was shifted 6 s to accommodate the delay in the BOLD response. The time-series images were then spatially normalized into Talairach space, an approach that has been validated in previous developmental studies (Burgund et al. 2002).

Selection of Functional ROIs

As in previous studies using this movie localizer task, we defined face-selective ROIs by the weighted contrast $[3 \times (\text{faces}) - (\text{objects} + \text{buildings} + \text{navigation})]$, and place-selective ROIs were defined as $[(\text{buildings} + \text{navigation}) - 2 \times (\text{faces})]$ because scenes of buildings and navigation both drive PPA activation (Hasson et al. 2004; Avidan et al. 2005; Scherf et al. 2007, 2010; Humphreys et al. 2008). In each participant, each contrast was computed on the z -transformed raw signal and was corrected for multiple comparisons using the false discovery rate procedure (Genovese et al. 2002) with $q < 0.10$. Each ROI was defined independently in each hemisphere in each individual.

We defined the measures of category selectivity with respect to all other categories. Note that these definitions are extremely conservative in that they identify many fewer voxels when compared with a contrast that would define each visual category against a fixation baseline. Critically, these contrasts identify nonoverlapping sets of voxels in all participants, indicating that they identify the most selective of voxels for each visual category.

The face-related ROIs included the set of contiguous face-selective voxels anywhere in the fusiform gyrus (FG; as determined by the maximal x , y , and z coordinates of BA 37 in the Talairach atlas), and separately in the region traditionally called the OFA. We did not consistently observe multiple FFA ROIs in this sample in response to this movie localizer task. In individual subjects for whom we did observe multiple ROIs in the fusiform, we took the one who was closest to the group level adult coordinates we have reported in the past ($40, -41, -21$).

The place-related ROI included the contiguous place-selective voxels in the parahippocampal gyrus (as determined by the maximal x , y , and z coordinates of BAs 34, 35, and 36 in the Talairach atlas). The ROIs were quantified in terms of the total number of active voxels (size), magnitude of category selectivity, and a measure of the variation in the coordinates of the centroid of activation from the centroid of activation of adult group-defined ROIs in another sample using the same movie localizer task (Scherf et al. 2007). These are the ROI measures that have been previously shown to exhibit developmental change across the age range of the participants in the current sample (Scherf et al. 2007, 2011; Golarai et al. 2010). If a participant did not have a definable ROI, a score of 0 was submitted for the size of the ROI and the subject was excluded from analyses that involved information about the magnitude of selectivity and the location of the ROI. Importantly, the number and age-related distribution of 0 volume scores was fairly consistent across the functional ROIs (rFG 7, lFG 8, rOFA 9, lOFA 12, rPPA 7, and lPPA 11).

To compute the magnitude of category selectivity within each ROI in each hemisphere, separate ROI-based GLMs were conducted for each participant who exhibited identifiable category-selective activation in each ROI. This generated beta weights for each condition (i. e., faces, places, buildings, navigation) for each participant. Face selectivity in the OFA and FFA was computed by submitting these beta weights to the following contrast: $[3 \times (\text{faces}) - (\text{objects} + \text{buildings} + \text{navigation})]$. Place selectivity in the PPA was computed by submitting these beta weights to the following contrast: $[(\text{buildings} + \text{navigation}) - 2 \times (\text{faces})]$. These difference scores were submitted as a predictor variable of tract property (i. e., volume, FA, MD, RD, and AD) in separate step-wise regressions with age as the first predictor variable.

To compute the variation in the coordinates of each ROI, we calculated the distance in stereotactic space between the midpoint of each individually defined ROI and the midpoint of the adult group-defined ROI in each individual as in our previous work (Scherf et al. 2010). For example, the midpoint of the adult group-defined face-selective right FG occurred at the coordinates ($40, -41, -21$). For a particular 7-year-old participant, the midpoint of his individually defined face-selective right FG ROI occurred at the coordinates ($33, -36, -16$), resulting in a distance of 9.9 mm, calculated as follows:

$$\sqrt{(7^2 + 5^2 + 5^2)} = 9.9$$

This procedure is roughly equivalent to computing the geometric mean of the differences between the 2 centroids of activation; however, it preserves the pooled distance in the original units (mm). This allowed us to simultaneously account for variation in all 3 directions of the centroid of activation for an individually defined ROI from a well-established adult group-defined ROI. These measures were then submitted to

Table 1Summary of regressions of macro- and microstructural tract measures with age ($N = 50$)

	RILF			LILF			RIFOF			LIFOF			F-Ma			F-Mi		
	F	r^2	P	F	r^2	P	F	r^2	P	F	r^2	P	F	r^2	P	F	r^2	P
Volume																		
Non-normalized	16.0	0.25	<0.0002	16.6	0.26	<0.0002	0.9	0.02	ns	0.5	0.01	ns	2.6	0.05	ns	0.6	0.01	ns
Normalized	10.3	0.18	<0.005	7.7	0.14	<0.008	0.0	0.0	ns	0.0	0.0	ns	0.0	0.0	ns	3.1	0.06	ns
Micro																		
FA	9.7	0.17	<0.005	3.2	0.06	ns	7.6	0.14	ns	0.7	0.01	ns	8.1	0.14	<0.008	6.3	0.12	ns
MD	35.4	0.42	<0.0001	31.0	0.39	<0.0001	15.6	0.25	<0.001	1.6	0.03	ns	11.6	0.19	<0.005	13.7	0.22	<0.001
RD	35.5	0.42	<0.0001	26.4	0.36	<0.0001	19.9	0.29	<0.0001	3.0	0.06	ns	12.1	0.20	<0.005	12.0	0.20	<0.005
AD	5.2	0.10	ns	5.3	0.10	ns	0.5	0.01	ns	0.3	0.00	ns	0.8	0.02	ns	6.6	0.12	ns

Bold P -values represent those that survived the Bonferroni correction of $P < 0.008$.

ILF: inferior longitudinal fasciculus; IFOF: inferior fronto-occipital fasciculus; F-Ma: forceps major; F-Mi: forceps minor; FA: fractional anisotropy; MD: mean diffusivity; RD: radial diffusivity; AD: axial diffusivity.

Table 2Summary of results from multiple regressions investigating relation between age, ROI size, and tract measures controlling for motion in the entire sample ($N = 35$)

	RILF				LILF				RIFOF				LIFOF							
	F	P	r^2 change	P_{Age}	$P_{ROI\ size}$	F	P	r^2 change	P_{Age}	$P_{ROI\ size}$	F	P	r^2 change	P_{Age}	$P_{ROI\ size}$	F	P	r^2 change	P_{Age}	$P_{ROI\ size}$
Non-normalized volume																				
FFA	8.6	<0.001	0.42	<0.008	<0.008	6.4	<0.001	0.41	<0.001	ns	1.3	ns				0.5	ns			
OFA	5.0	<0.001	0.28	<0.005	ns	6.3	<0.001	0.41	<0.001	ns	1.3	ns				0.5	ns	0.5	ns	0.5
PPA	4.9	<0.005	0.28	<0.005	ns	8.3	<0.001	0.48	<0.001	<0.05	1.1	ns				0.4	ns			
Normalized volume																				
FFA	6.6	<0.001	0.39	<0.025	<0.01	4.7	<0.005	0.34	<0.005	ns	1.2	ns				0.4	ns			
OFA	4.2	<0.01	0.28	<0.01	ns	4.3	<0.008	0.32	<0.005	ns	1.2	ns				0.4	ns			
PPA	3.7	<0.025	0.25	<0.005	ns	5.5	<0.005	0.38	<0.005	ns	1.0	ns				0.2	ns			
Microstructural indices																				
FA																				
FA	1.8	ns				0.9	ns				2.3	ns				1.3	ns			
MD	6.2	<0.001	0.28	<0.025	ns	3.1	<0.05	0.26	<0.01	ns	3.4	<0.025	0.12	<0.05	ns	3.1	<0.05	.26	<0.01	ns
RD	7.4	<0.001	0.26	<0.025	ns	3.9	<0.025	0.25	<0.01	ns	3.7	<0.025	0.16	<0.05	ns	3.9	<0.025	.25	<0.01	ns
OFA																				
FA	1.6	ns				0.8	ns				2.2	ns				1.4	ns			
MD	4.6	<0.005	0.21	<0.008	ns	3.1	<0.05	0.26	<0.005	ns	3.4	<0.025	0.11	ns	ns	1.1	ns			
RD	6.1	<0.001	0.21	<0.008	ns	4.1	<0.01	0.25	<0.005	ns	3.8	<0.025	0.17	<0.05	ns	2.0	ns			
PPA																				
FA	2.1	ns				1.0	ns				2.3	ns				0.8	ns			
MD	4.6	<0.005	0.21	<0.008	ns	3.0	<0.05	0.25	<0.005	ns	3.4	<0.025	0.11	ns	ns	1.2	ns			
RD	6.4	<0.001	0.23	<0.01	ns	3.8	<0.025	0.24	<0.008	ns	3.8	<0.025	0.17	<0.05	ns	1.2	ns			

Note: Full model for each regression included 2 motion factors, age, and ROI size with the following degrees of freedom (4, 29). r^2 change represents the additional variance accounted for in the model by the factors of interest (age, ROI size) after accounting for motion in both the y - and z -directions. In addition, regressions were all run within the hemisphere (e.g., the size of right FG ROI predicting the volume of right ILF). Bold P -values represent those that survived the Bonferroni correction of $P < 0.008$.

ILF: inferior longitudinal fasciculus; IFOF: inferior fronto-occipital fasciculus; FA: fractional anisotropy; FFA: fusiform face areas; OFA: occipital face area; PPA: parahippocampal place area; MD: mean diffusivity; RD: radial diffusivity.

correlational analyses with the measures of macro- and microstructural properties of the fiber tracts of interest.

Statistical Analyses

To evaluate age-related differences in the structural properties of the tracts of interest, both the volume (in cubic millimeters) and microstructural indices were submitted to separate linear regressions with age as the independent factor, separate for each tract in each hemisphere. The volume measure included the total number of voxels through which the fiber tract passed, multiplied by the voxel volume ($1.6 \times 1.6 \times 3.0$ mm). We also computed the normalized volume for each tract as a proportion of the whole-brain volume to accommodate for individual differences and age-related differences in whole-brain volume. The microstructural measures included the mean FA, MD, RD, and AD across all the voxels through which the tracts passed.

To evaluate relations between the emerging functional profile of category-selective ROIs and the structural properties of the tracts of interest, we used the functional measures of the ROIs as predictors in a step-wise regression with age as the primary predictor on the volume and microstructural indices of each tract separately within each hemisphere. For example, the size, magnitude of face selectivity, and variability in locus of the right FFA were each used to predict the tract volume, as well as the mean FA and diffusivity values, in the right ILF and IFOF as well as the F-Ma and F-Mi. We included motion along the y - and z -axis as covariates in these analyses since motion changed significantly ($P < 0.05$) with age along these 2 dimensions in this sample.

Results

Using the data from both structural and functional imaging, we explored 2 main issues: The presence of age-related

Table 3Summary of results from multiple regressions investigating relation between age, ROI size, and tract measures controlling for motion in individuals between the ages of 6–15 years ($N = 24$)

	RILF					LILF					RIFOF					LIFOF				
	F	P	r ² change	P _{Age}	P _{ROI size}	F	P	r ² change	P _{Age}	P _{ROI size}	F	P	r ² change	P _{Age}	P _{ROI size}	F	P	r ² change	P _{Age}	P _{ROI size}
Non-normalized volume																				
R FFA	4.2	<0.025	0.30	<0.05	ns	2.7	ns				1.0	ns				1.1	ns			
R OFA	3.7	<0.05	0.28	<0.01	ns	2.9	<0.05	0.05	ns	ns	0.9	ns				1.1	ns			
R PPA	3.8	<0.025	0.28	<0.01	ns	4.3	<0.025	0.15	ns	<0.05	0.9	ns				1.1	ns			
Normalized volume																				
R FFA	3.0	<0.05	0.26	ns	ns	2.2	ns				0.8	ns				0.8	ns			
R OFA	2.6	ns				2.2	ns				0.7	ns				0.9	ns			
R PPA	2.8	ns				3.5	$P < 0.05$	0.12	ns	ns	0.8	ns				0.8	ns			
Microstructural indices																				
FFA																				
FA	0.9	ns				0.6	ns				1.2	ns				0.4	ns			
MD	7.2	<0.001	0.46	<0.005	ns	6.6	<0.005	0.43	<0.001	ns	4.9	<0.008	0.14	<0.05	ns	1.4	ns			
RD	4.8	<0.01	0.30	<0.025	ns	4.6	<0.01	0.31	<0.01	ns	2.3	ns				1.3	ns			
OFA																				
FA	0.6	ns				1.4	ns				1.2	ns				0.4	ns			
MD	6.6	<0.005	0.43	<0.001	ns	4.6	<0.01	0.46	<0.005	ns	4.9	<0.008	0.14	<0.05	ns	1.2	ns			
RD	4.6	<0.01	0.31	<0.01	ns	4.7	<0.01	0.43	<0.005	ns	2.3	ns				1.0	ns			
PPA																				
FA	0.8	ns				1.7	ns				1.3	ns				0.4	ns			
MD	6.5	<0.005	0.42	<0.001	ns	4.7	<0.01	0.46	<0.005	ns	4.9	<0.008	0.14	<0.05	ns	2.1	ns			
RD	4.5	<0.01	0.30	<0.008	ns	5.1	<0.008	0.45	<0.005	ns	2.5	ns				1.2	ns			

Note: Full model for each regression included 2 motion factors, age, and ROI size with the following degrees of freedom (4, 18). r^2 change represents the additional variance accounted for in the model by the factors of interest (age and ROI size) after accounting for motion in both the y- and z-directions. In addition, regressions were all run within the hemisphere (e.g., the size of right FG ROI predicting the volume of right ILF). Bold P -values represent those that survived the Bonferroni correction of $P < 0.008$.

ILF: inferior longitudinal fasciculus; IFOF: inferior fronto-occipital fasciculus; FA: fractional anisotropy; FFA: fusiform face areas; OFA: occipital face area; PPA: parahippocampal place area; MD: mean diffusivity; RD: radial diffusivity.

differences in the white matter tracts that connect regions within the face network, and the existence of associations between the emerging structural properties of these tracts and profile of functional activation within face-selective regions. Tables 1–3 contain the entire set of results from the regression analyses of age and ROI size with the volume and microstructural indices of the tracts of interest, separately in each hemisphere, for the entire sample (Tables 1 and 2) and for the children and adolescents (individuals ages 6–15 years; Table 3).

Age-Related Differences in White Matter Tracts

To maintain the family-wise error rate in this large number of analyses, we employed a Bonferroni correction, with a corrected value of $P < 0.008$ (0.05/6), taking into consideration the 6 age-related regressions computed separately for each tract.

Inferior Fronto-Occipital Fasciculus

Neither the right nor the left IFOF exhibited an age-related increase in volume, even when the tract volume was normalized by the total white matter volume in each participant (Table 1 and Fig. 2). However, there were significant age-related improvements in the microstructural properties of the tracts, particularly within the right IFOF. The MD, $F_{1,48} = 15.6$, $P < 0.0003$, and RD, $F_{1,48} = 19.9$, $P < 0.0001$, but not the AD or FA ($P = ns$), showed dramatic decreases with age in the right IFOF. There were 4 participants (1 adult, 2 adolescents, and 1 child) who had no identifiable streamlines in the right IFOF, and the findings remained the same even when these 4 participants were removed from the analyses. These findings are consistent with studies reporting age-related changes in the microstructural properties of the right IFOF (Lebel et al. 2008;

Lebel and Beaulieu 2011). The left IFOF did not exhibit this age-related improvement in microstructural properties (Table 1). There were 8 participants who did not have identifiable streamlines in the left IFOF (1 adult, 4 adolescents, and 3 children), and the pattern of results also remained unchanged when these participants were removed from the analyses.

Importantly, the inability to identify streamlines in a subset of participants does not imply that the fiber tracts do not exist in these individuals. Our multiple ROI approach for defining the streamlines is quite rigorous (i.e., streamlines were only extracted if they passed through both ROIs in both directions and were not included in another tract) and was designed to maximize the recovery of streamlines within tracts while safeguarding against identifying spurious streamlines; this conservative approach may have prevented us from identifying streamlines in some individuals, particularly in the longer tracts, like the IFOF. Specifically, 8 of the total 50 participants did not have identifiable streamlines in the left IFOF, which is 16% of the sample. However, all of these participants exhibited measurable macro- and microstructural indices in all other tracts that were within 2 SD of the mean of the sample (computed without these participants), suggesting that the inability to define IFOF streamlines within these individuals was not likely due to a global signal quality problem in these individuals. The left IFOF is also difficult to track even with a 64-direction DTI protocol in typically developing adults. Thiebaut de Schotten et al. (2011) reported higher individual variability in the number of identifiable streamlines in the left than the right IFOF even in healthy young adults.

Inferior Longitudinal Fasciculus

There were marked age-related differences bilaterally in the volume and microstructural properties of the ILF. In both

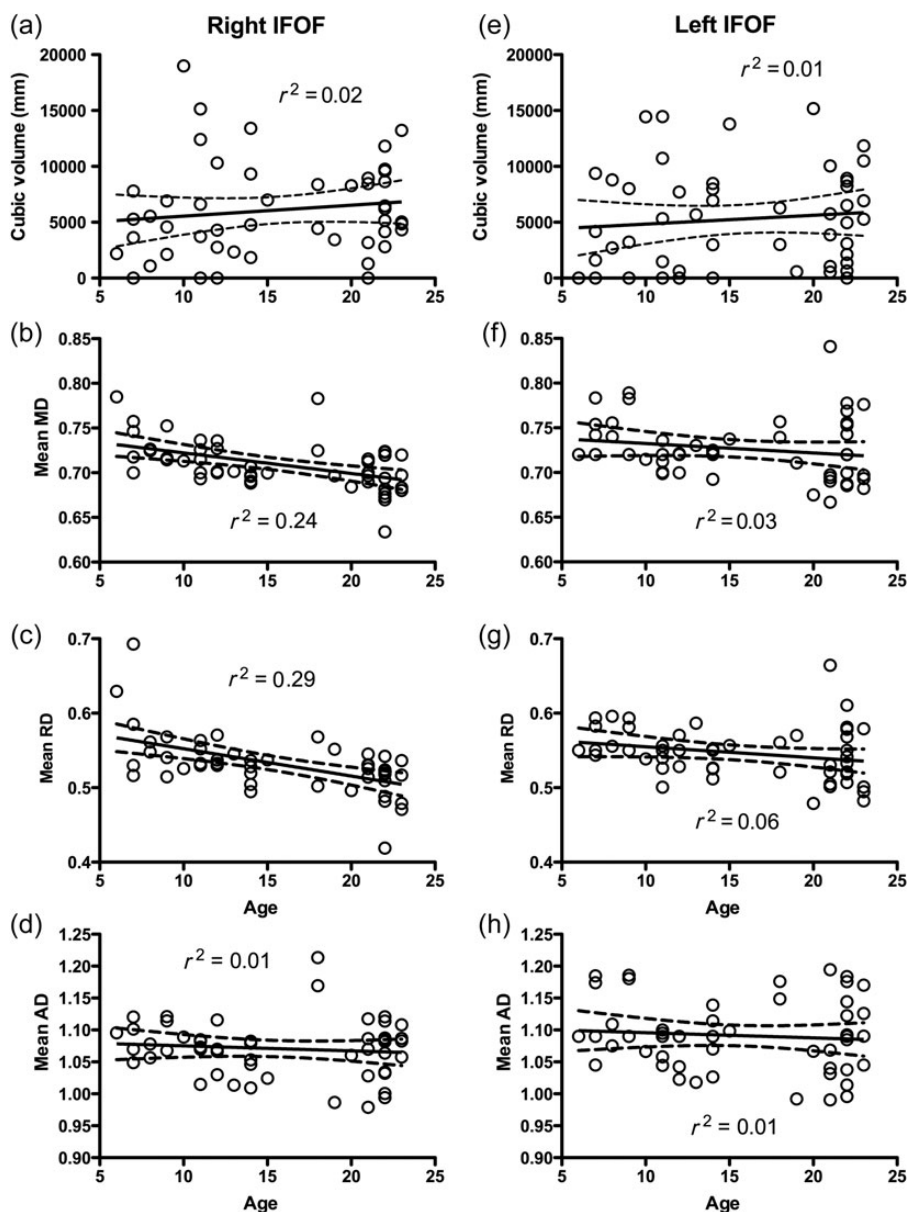


Figure 2. Analyses of age-related differences in the macro- and microstructural properties of the IFOF. The volume of both the right (3a) and left (3e) IFOF as indexed by the mean cubic volume within the fasciculus, did not vary as a function of age. However, there were significant age-related differences in the microstructural properties of the right IFOF. Specifically, the MD (3b) and RD (3c) decreased with age. In contrast, the AD (3d) was stable across the age range.

hemispheres, the number of voxels in the ILF increased significantly with age (Fig. 3*a,e*) (right: $F_{1, 48} = 16.0$, $P < 0.0002$; left: $F_{1, 48} = 16.6$, $P < 0.0002$). These age-related increases in volume were also observed when the ILF volume was normalized by the whole-brain volume for each subject (Table 1). At the microstructural level, the mean FA increased in the right ILF, $F_{1, 48} = 9.7$, $P < 0.005$, but did not reach significance at the corrected P -value in the left ILF, $F_{1, 48} = 3.2$, $P = ns$. Importantly, both the MD and RD significantly decreased with age in the right and left ILF, while the AD was stable across the age range in both hemispheres (Fig. 3 and Table 1). One participant did not have any identifiable streamlines in the right ILF; removal of this participant did not affect the findings. All participants had identifiable streamlines in the left ILF. Together, these findings uncover strong age-related increases

in volume and microstructural properties in the ILF in both hemispheres.

Forceps Major

All participants had identifiable streamlines in the F-Ma. The volume of the F-Ma did not change with age in this sample, $F_{1, 48} = 2.6$, $P = ns$, even when the tract volume was normalized for whole-brain volume for each participant, $F_{1, 48} = 0.0$, $P = ns$. However, the F-Ma did exhibit significant age-related improvement in some of its microstructural properties, including mean FA: $F_{1, 48} = 8.1$, $P < 0.008$, MD: $F_{1, 48} = 11.6$, $P < 0.002$, and RD: $F_{1, 48} = 12.1$, $P < 0.002$, but not AD: $F_{1, 48} = 0.8$, $P = ns$. These findings are consistent with the idea that the streamlines in the F-Ma are becoming increasingly myelinated during this age range.

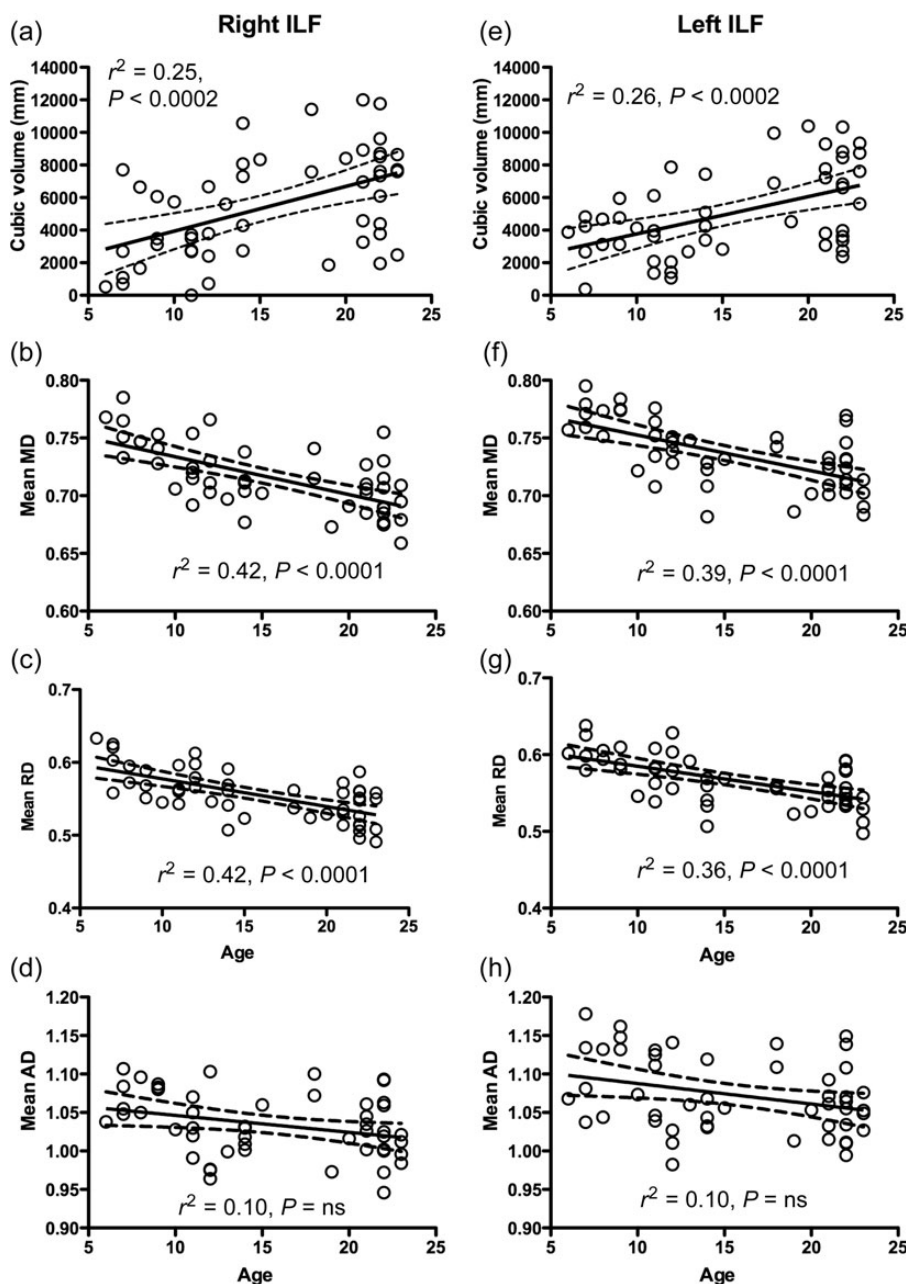


Figure 3. Age-related differences in the macro- and microstructural properties of the ILF. The volume of both the right (a) and left (e) ILF, as indexed by the mean cubic volume within the fasciculus, increased significantly with age. Similarly, the microstructural properties of the ILF exhibited age-related differences, such that the MD and RD decreased significantly with age in both the right (b and c) and left (f and g) hemispheres. In contrast, the AD was stable across the age range (d and h). This pattern of results suggests that the right and left ILF are becoming increasingly more myelinated with age.

Forceps Minor

All participants also had identifiable streamlines in the F-Mi. As in the F-Ma, the volume of the F-Mi did not change with age in this sample, $F_{1, 48} = 0.6$, $P = \text{ns}$. However, both the MD, $F_{1, 48} = 13.7$, $P < 0.001$, and RD, $F_{1, 48} = 12.0$, $P < 0.005$, significantly decreased with age, while the AD was stable across this age range (Table 1), suggesting that the F-Mi is becoming increasingly myelinated across adolescence as well.

Comparing Age-Related Differences Across Tracts

To contrast the patterns of age-related differences across tracts, the slopes and intercepts of the regression lines were

compared for each pair of tracts within hemisphere (e.g., right ILF vs. right IFOF volume) in separate analyses of covariances. The slopes of the regressions of age on tract volume only tended to differ between the ILF and IFOF in the right hemisphere, $F_{1, 96} = 2.9$, $P = 0.09$. No other tracts exhibited significantly different slopes in the regressions of tract volume on age (i.e., pattern of age-related change). However, the right and left ILF, as well as the right and left IFOF, all exhibited significantly lower intercepts than both the F-Ma and F-Mi, indicating that the 2 control tracts had larger volumes than the ILF and IFOF in the youngest children (all $P < 0.001$). With respect to the microstructural indices, the left hemisphere ILF and IFOF

differed in the pattern of age-related differences (e.g., slopes of regression lines) across participants in MD, $F_{1, 96} = 4.1$, $P < 0.05$, but only tended to differ in RD, $F_{1, 96} = 2.9$, $P = 0.09$, indicating a steeper decline in these measures in the left ILF than in the left IFOF. Finally, the intercepts of the regression lines were also different in the left ILF and IFOF for RD, $F_{1, 97} = 10.0$, $P < 0.005$, indicating higher RD in the youngest children in the IFL compared with the IFOF. In summary, adult-like volume in the right IFOF is evident sooner (i.e., in younger individuals) than in the right ILF, and the diffusivity parameters associated with myelination are higher and decrease faster in the left ILF than in the left IFOF.

Age-Related Differences in Functional ROIs

As in previous studies (Scherf et al. 2007, 2011), we evaluated age-related differences in the profile of functional activation in several face- and place-related ROIs in the subset of 35 individuals for whom we acquired functional data. We ran separate regressions of age on ROI size, magnitude of selectivity, and location for each ROI in each hemisphere separately.

Fusiform Gyrus Face-Related ROIs

Consistent with our previous findings (Scherf et al. 2007), both the right, $F_{1, 33} = 5.4$, $P < 0.05$, and the left, $F_{1, 33} = 6.2$, $P < 0.025$, face-selective ROIs in the FG increased in size with age. When the motion covariates for the y - and z -directions were included in the models, the full model including age and motion covariates was no longer significant in either the right, $F_{3, 30} = 1.6$, $P = \text{ns}$, or the left FG ROIs, $F_{3, 30} = 1.9$, $P = \text{ns}$; in spite of this, age remained a weak, but significant predictor of the size of both the right ($r^2 = 0.14$, $P = 0.05$) and left ($r^2 = 0.17$, $P < 0.05$) FG ROIs.

The magnitude of selectivity did not change across the age range in either the right, $F_{1, 27} = 2.3$, $P = \text{ns}$, or left, $F_{1, 26} = 1.3$, $P = \text{ns}$, FG ROIs. This was also the case when the motion covariates were included in the model. Age did not predict differences in the magnitude of selectivity within the right FG ROI. Finally, the right FG ROI only showed a trend toward a significant effect of age in the analysis of the locus of activation, $F_{1, 26} = 3.4$, $P = 0.08$, suggesting that the variability in the centroid of the right face-related FG ROI tends to be reduced with age. However, when the motion covariates were included in the model, age was no longer predictive of the locus of activation in the right FG.

Occipital Face Area

As in the fusiform gyrus, the right, $F_{1, 33} = 6.5$, $P < 0.025$, and left, $F_{1, 33} = 14.4$, $P < 0.001$, OFA ROIs increased in size with age. Similarly, when the motion covariates were included in the models, the full model was no longer significant for the right OFA, $F_{3, 30} = 1.9$, $P = \text{ns}$, but did remain significant for the left OFA, $F_{3, 30} = 4.6$, $P < 0.01$. Importantly, age remained a significant predictor of both right ($r^2 = 0.17$, $P < 0.05$) and left ($r^2 = 0.26$, $P < 0.005$) OFA size.

In addition, the magnitude of selectivity for faces did not change across the age range in either the right, $F_{1, 24} = 2.4$, $P = \text{ns}$, or the left, $F_{1, 21} = 3.6$, $P = \text{ns}$, OFA ROIs, even when the motion covariates were included in the model. Finally, the variability in the locus of activation of the OFA did not change with age in either hemisphere ($P > 0.25$).

Parahippocampal Place Area

Finally, only the right, $F_{1, 33} = 8.3$, $P < 0.01$, but not the left, $F_{1, 33} = 2.8$, $P = \text{ns}$, PPA ROI increased in size with age. The effect of age ($r^2 = 0.14$, $P < 0.05$) on the size of the right PPA remained significant after the motion covariates were included in the regression, $F_{3, 30} = 3.6$, $P < 0.025$. The PPA did not exhibit an increase in the magnitude of selectivity for places in either the right, $F_{1, 26} = 0.0$, $P = \text{ns}$, or the left, $F_{1, 27} = 0.1$, $P = \text{ns}$, hemispheres with age. Also, the variability in the locus of activation of the PPA did not change with age in either hemisphere ($P > 0.25$).

Structure–Function Relations Between Tract Properties and Functional ROIs

Given that there were age-related increases in the size of many functionally defined ROIs as well as in the structural properties of the fiber tracts that connect these ROIs to each other, we were interested in evaluating emerging structure–function relations between the ROIs and fiber tracts. To do so, we computed step-wise regression analyses of the size, magnitude of selectivity, and locus of each of the functional ROIs (FFA, OFA, and PPA) on the volume, mean FA, MD, RD, and AD of each of the tracts (within each hemisphere) with age as the primary predictor. Recall that face selectivity in the OFA and FFA was computed by submitting these beta weights to the following contrast: [$3 \times (\text{faces}) - (\text{objects} + \text{buildings} + \text{navigation})$]; and place selectivity in the PPA was computed by submitting these beta weights to the following contrast: [$(\text{buildings} + \text{navigation}) - 2 \times (\text{faces})$].

We included the motion in both the y - and z -axis as covariates in all the analyses, so that any structure–function relations could only be significant after controlling for motion. To maintain the family-wise error rate in these analyses, we used a Bonferroni correction on significant P -value within each fiber tract of ($0.05/6 = 0.008$). We computed these regressions with age as the first predictor in a step-wise fashion to determine the relative and potentially separate contributions of age and ROI measures as factors in emerging function–structure relations. For each of the significant correlations resulting from the regression analyses, we evaluated the robustness of the correlation in separate bootstrap analyses using 1000 iterations.

Despite the age-related changes in the structural properties of the right and left IFOF as well as the F-Ma and F-Mi, these changes were not significantly related to the functional characteristics of any of the ROIs. The only significant structure–function relations were observed in the ILF, which are described below. Furthermore, these relations were only observed between the functional characteristics of the FFA (and not any other ROI) and the ILF. Table 2 illustrates the results of these analyses in the full sample of participants. We also performed the same analyses on the children and adolescents, without the inclusion of adults, to evaluate the strength of age-related differences that are not anchored to adult levels of functional activation or structural properties of the fiber tracts. These additional analyses are represented in Table 3.

ROI Size

The right ILF was the only tract in which a significant relation emerged between the size of the face-related ROIs and the indices of tract architecture. The Pearson correlation

coefficient between the size of the right FFA and the volume of the right ILF was $r = 0.58$, with 99% confidence intervals (CIs) based on 1000 bootstraps of 0.38/0.81, which is different from 0 at $P < 0.01$. When we eliminated the participants with no definable right FG in the analysis, the correlation was still significant ($r = 0.32$, 99% CIs of 0.07/0.57, which is different from 0 at $P < 0.01$).

The step-wise regression with both age and size of the ROI was also significant in the right hemisphere, $F_{4, 29} = 8.6$, $P < 0.001$ (r^2 change = 0.415). In other words, after controlling for motion, an additional 41.5% of the variance in the volume of the right ILF was accounted for by the age of participants and the volume of the right FFA. Age ($P < 0.008$) and right FFA volume ($P < 0.008$) were independent significant predictors of the volume of the right ILF even after accounting for the slight differences in motion in the y - and z -directions (Fig. 4), such that older individuals as well as those with larger functionally defined FFA ROIs exhibited larger volume in the right ILF. This relation between right FG size and normalized volume for the right ILF volume was nearly significant as well (Table 2).

Importantly, even in the children and adolescents alone, the correlation between right FG size and right ILF volume is significant ($r = 0.47$, 95% CIs 0.22/0.73, $P < 0.001$). However, the change in age dominates this relation. The step-wise regression with both age and the size of the right FG was significant, $F_{4, 18} = 4.2$, $P < 0.025$, with an r^2 change = 0.303 (after controlling for motion); however, while age remained a significant predictor of the volume of the right ILF ($P < 0.05$), the size of the right FFA ($P = \text{ns}$) did not (Table 3). In contrast, there were no significant relations between tract measures and functional ROI measures in the adults alone. We also ran the structure–function correlations separately on the children (6–11 years) and adolescents (12–15 years). There were no significant structure–function relations in either group. However, we may not have enough power to detect such structure–function relations in these subgroups of participants. This pattern of findings indicates that the age-related changes in this function–structure relation continue to progress from adolescence to early adulthood.

There were no other significant relations between the size of any of the remaining ROIs (i.e., left FFA, right/left OFA, right/left PPA) and tract measures (volume or diffusivity) in any of the other tracts (i.e., left ILF, right/left IFOF, F-Mi, F-Ma). All other relations between ROI size and tract integrity were mediated by age (Fig. 4 and Tables 2–3).

Finally, it is important to note that, with the exception of the left FFA size, the size measures of the functionally defined ROIs were all normally distributed with a slight positive skew, due in large part to the small volume ROIs in many of the young individuals. The tract volumes were all normally distributed as well, indicating that there was not disproportionately more variance in the right FFA size and the right ILF volume across participants compared with the other measures. We transformed the left FFA size measure using the natural log transformation, which normalized the distribution, and the pattern of results did not change. There was no relation between the size of the left FFA and the volume of the left ILF after controlling for motion and taking age into account. These findings provide support for the notion that there was comparable variability across all measures, and so it is not the case that increased variability in some tract might have permitted the identification of age trends and function–structure relations independent of age.

ROI Magnitude of Selectivity

The magnitude of selectivity in each ROI failed to predict both macro- and microstructural indices of any tract.

ROI Location

Given that the right FFA was the only ROI that exhibited weak age-related differences in its locus with age, we evaluated whether this emerging stabilization in the locus of the right FFA was related to the architecture of the fiber tracts that receive input from the FFA, or whether age predicted all the variance in both the locus of the right FFA and the properties of the fiber tracts. The step-wise regression with age as the first predictor and right FFA distance (from a group ROI defined by a separate set of adults) as the second predictor was not significant, $F_{4, 22} = 1.9$, $P = \text{ns}$, after controlling for motion. Variation in the locus of the right FFA did not predict the volume (or any microstructural measure) of the ILF independently from age ($P = \text{ns}$).

In summary, from the multitude of analyses investigating age-related differences in structure–function relations, only a single, selective relation emerged between the volume of the right ILF and the volume of the right FG face-selective ROI. This was true even after controlling for the minimal differences in motion. In all other significant results, age was the only factor that predicted specific tract properties, including both macro- and microstructural properties and functional properties of the ROIs. Importantly, these age-related effects were present in the analyses of the entire sample, as well as in the subset of participants for whom we had functional data and could control for motion differences across the age range. Together, these findings lend strong support to the notion that the observed age-related effects were not spurious or fundamentally related to age-related differences in motion.

Discussion

The central question guiding this work concerns how a complex distributed neural network emerges and becomes functionally integrated over the course of development. Specifically, we measured age-related differences in the “structural properties of the fiber tracts” connecting the multifocal nodes of the neural circuitry supporting face perception (ILF and IFOF) and evaluated whether the emergence of efficient functional organization within this network is related to such structural differences.

Importantly, we replicated and extended existing findings about age-related differences in the structural properties of the tracts of interest. All tracts, with the exception of the left IFOF, exhibited age-related improvements in their microstructural properties, evincing a significant decrease in mean and radial, but not axial, diffusivity from childhood to early adulthood. This result is consistent with the idea that the increasingly restricted diffusion perpendicular to the axons in these tracts reflects continued myelination from childhood through early adulthood. The left IFOF exhibited stable levels of microstructural properties across the age range, indicating that it may be a very early developing fiber tract, which has not been previously reported. However, this pattern of early stabilization of the left IFOF should be interpreted with caution, given that this tract was particularly hard to identify in some participants (including children, adolescents, and adults).

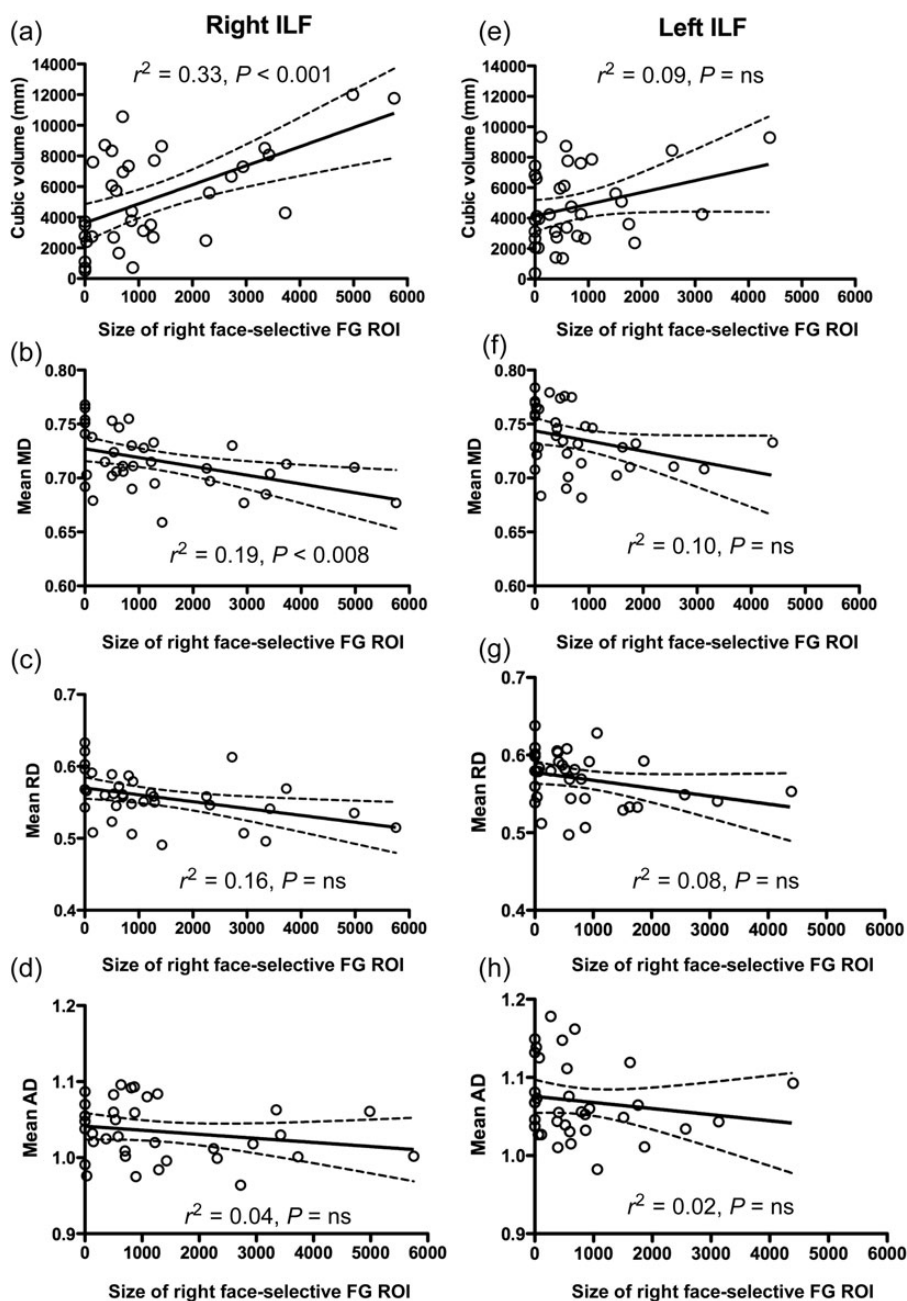


Figure 4. Relation between structural properties of the right ILF and larger functionally defined face-selective regions in the fusiform gyrus. The volume of the right ILF was related to the size of the right functionally defined face-selective ROI in the fusiform gyrus (a). Similarly, as the mean and RD of the right ILF decreased, indicating increasing myelination of the tract, the size of the right hemisphere functionally defined face-selective ROI in the fusiform gyrus increased (b and c). In contrast, the AD in the right ILF was not related to the size of the functionally defined face-selective ROI in the fusiform gyrus (d). These same structure–function relations did not exist in the left hemisphere (e, f, and g).

Although the right IFOF exhibited an increase in microstructural integrity, it did not increase in volume. This pattern of results may reflect an increase in myelination of the fibers in the IFOF, but not to the extent that it results in an increase in volume. At the macrostructural level, only the ILF exhibited an age-related change in volume, which was evident in both hemispheres, and this held even when the volume of the ILF was normalized for each participant based on the total white matter volume in the whole brain and in the subset of participants for whom we could control for motion during the functional scan. These findings of increases in both the microstructural integrity as well as the volume of the right ILF

are consistent with recent longitudinal work (Lebel and Beaulieu 2011) and suggest that the ILF is becoming increasingly myelinated and/or more densely packed with axons with age (Beaulieu 2002; Song et al. 2005; Lebel and Beaulieu 2011). However, it is important to note that we report this finding in the context of having employed a novel approach for considering potential motion differences across the age range (i.e., using motion measures from a separate functional scan as a proxy for motion in the DTI scan). Including motion estimates from the functional scan as covariates in the regressions of age-related differences in tract measures actually improved the amount of variance that was accounted for by age in these

analyses. We suggest that this may be a useful strategy for considering potential motion differences in developmental DTI studies in the future, and particularly for those studies including very young participants.

This differential pattern of results raises the question about why some tracts, like the ILF, take longer to reach adult-like architecture in comparison with other tracts, like the IFOF. The ILF–IFOF contrast is particularly interesting because the IFOF is longer than the ILF and innervates the prefrontal cortex, which demonstrates prolonged structural development (Gogtay et al. 2004), yet the ILF follows a more protracted developmental course. These results challenge the idea that the process of myelination necessarily follows a posterior-to-anterior gradient during development (Yakovlev and Lecours 1967) and provokes further consideration about the developmental determinants of white matter integrity.

Emerging Function–Structure Relations

Given the pattern of developmental differences in the tracts documented here, 2 immediate questions arise. The first concerns the mechanism by which the white matter tracts change with age and the second concerns the relationship between these changes and alterations in functional characteristics of regions comprising the face circuit.

Having identified the structural changes that potentially contribute to circuit organization, we explored, in parallel, concomitant differences in the functional profile of face-related cortical regions, and then examined the joint structure–function correspondences. Using BOLD fMRI signals, we evaluated relations between the size, magnitude of selectivity, and location of regions of functional activation (i.e., OFA and FFA) that transmit signals via the tracts of interest (i.e., ILF and IFOF). We found a highly selective result. Across the full age range, individuals with larger right FFA volumes also exhibited larger right ILF volumes. Neither the right OFA nor the right PPA exhibited this structure–function relation with the right ILF. This is important given that the OFA was functionally defined using the same contrast as was the FFA, suggesting that the functional definition of the contrast was not selectively biased to uncover a structure–function relation with the ILF. Secondly, given that the functional contrast for identifying the PPA was essentially the inverse of the definition of the FFA and OFA, it is important that we did not observe a significant structure–function relation between the PPA and the ILF in the reverse direction of the FFA–ILF relation. In addition, this pattern of results reflects the high degree of selectivity in the structure–function relations that we uncovered in this network.

Interestingly, this structure–function relation between the right FFA and right ILF was also present in just the children and adolescents (aged 6–15). However, once age was accounted for in the same model as size of the right FFA in the children and adolescents, the age effects on the volume of the ILF swamped all the significant variation, even though the size of the right FFA increased significantly across this age range. Additionally, we did not observe a significant relation between size of the right FFA and any of the diffusivity parameters of the right ILF, above and beyond the effects of age on these microstructural indices of this tract. Together, these findings indicate that age is the predominant factor influencing the volume of the right ILF during early development, during which time the right FFA grows significantly as well. One

interpretation of these findings is that the neural activity generated by larger functional regions may require and/or influence the development of larger fiber tracts (via increasing myelination of existing axons and/or more densely packed axons) to support the transmission of neural signals emanating from such regions. Interestingly, this pattern of results is not consistent with arguments, suggesting that functional brain development primarily proceeds by reducing highly distributed networks to become increasingly more focalized (smaller, fewer, and more dedicated regions supporting the behavior) with age (e.g., Durston et al. 2006). While this account may accurately characterize age-related changes in some neural systems, it does not apparently account for the age-related increases we see in the neural circuitry supporting face processing.

Importantly, we did not observe a similar structure–function relationship between the size of the left FFA, right or left OFA, or right or left PPA and any tract measures in the left ILF, right or left IFOF, F-MA, or F-Mi. Similarly, neither the magnitude of activation nor the locus of coordinates in any functional ROI was related to tract measures. This is not surprising given that in the existing studies evaluating age-related differences in the magnitude of activation within the ventral visual pathway that define functional ROIs at the individual level, there are no age-related differences in face-selectivity (e.g., Golarai et al. 2007, 2010; Scherf et al. 2007, 2011). This speaks to the highly selective nature of the dynamic changes that we observed in the relation between structural and functional development of a complex distributed neural system. Part of the reason that we observed this relation between the right FFA and the right ILF may be the tremendous developmental growth that exists in the size of the right FFA and the volume of the right ILF that is not observed in other regions or tracts and that may, therefore, provide a unique opportunity to test these emerging function–structure relations, particularly during the course of development.

To our knowledge, this is the first report of developmentally emerging relations between the properties of functional nodes of a circumscribed network and the structural connections between those nodes. There are a small number of developmental studies that have reported significant correlations between FA values and fMRI BOLD measures in whole-brain analyses of children engaging in working memory tasks (Olesen et al. 2003) as well as age-related differences in both structural and functional connectivities within targeted connections of the default mode network during rest (Supekar et al. 2010; Uddin et al. 2011). Surprisingly, these studies report that resting-state functional connectivity, that is temporal synchrony in functional activation between neural ROI during rest, can reach adult-like levels despite weak or non-existent structural connectivity between these same regions (Supekar et al. 2010; Uddin et al. 2011). These findings reflect the notion that, during development, there is a very complicated relationship between the functional and structural components of emerging neural circuits. Our findings elucidate the dynamic macro- and microstructural and functional age-related differences that characterize a circumscribed functional network, but they also have implications for how development and optimization of cortical organization might occur more generally. One possibility is that as functional cortical areas grow in size developmentally and vary in size across individuals even in adulthood, they may influence the structural

properties of the fiber tracts transmitting neural signals to and from these regions. Recent evidence in adults supports this notion of a very close, and even direct, relationship between functional patterns of activation in an individual's right fusiform gyrus and their own patterns of structural connectivity that define the input–output relations of the fusiform gyrus (Saygin et al. 2011).

This study represents a first step in uncovering the dynamics of emergent structure–function relations in the developing brain. Our cross-sectional design provided novel evidence of age-related differences (and hint at age-related changes) in these relations, but it is imperative that longitudinal designs be employed to understand, at closer range, the dynamics of these emergent structure–function relations within individuals. This latter approach will provide a clearer understanding of the causal mechanisms that shape these critical structure–function dynamics and the directionality of the developmental influence between brain structure and function, in particular. A complete understanding of the functional consequences of emerging structure–function relations in brain development will also need to include an assessment of how behavior is affected. Given that there is some empirical support for an existing relation between face identity recognition and the size of the FFA developmentally (Yovel et al. 2008; Golarai et al. 2010), we hypothesize that this component of face processing might be correlated with the observed structure–function relation we report.

Mechanistic Explanations for the Emerging Structure–Function Relations

Our findings of a dynamic association between emerging structural and functional architecture in the developing brain may provide important clues about the mechanisms by which neural circuits become organized and optimized in the human cortex. Previous work has provided evidence of activity-dependent mechanisms that promote myelination, suggesting that experience may influence myelination and thus, induce changes in diffusion parameters. For example, neural activity induces myelination both in vivo and in vitro in mice (Demerens et al. 1996). Rearing mice in darkness also reduces the rate of myelination of the optic nerve (Gyllenstein and Malmfors 1963). Recent human DTI studies consistently implicate experience-dependent plasticity in white matter tracts. For example, Bengtsson et al. (2005) found significant correlations between the number of hours children, adolescents, and adults practice playing piano and FA values in specific regions of the corpus callosum and internal capsule. These authors argued that long-term training can induce regionally specific plasticity in the myelination of tracts that are still developing, particularly during childhood. Several training studies with adults provide more direct evidence of experience-related changes in white matter properties, although the robustness of this evidence has been questioned (Thomas and Baker 2012). Young adults learning a second language exhibit progressive organizational changes in the white matter tracts associated with traditional left hemisphere language areas and their right homologs (Schlegel et al. 2012). Similarly, both younger and older adults exhibited an increase in the macro- and microstructural properties of the genu of the corpus callosum, compared with age-matched control participants after undergoing 100 h of training in working memory, episodic memory, and perceptual speed tasks (Lövdén et al. 2010). The implication of these findings for

the current study is that extensive experience with faces over the course of development might lead to increasing activation within face-related neural regions that serves as a trigger for the specific refinement of the white matter tracts in this circuit.

We have emphasized the directionality of functional to structural changes in shaping the development of the face-processing network; however, it may also be that increasing the integrity of the structural architecture of fiber tracts increases the propagation of neural signal throughout the circuit, thereby enhancing the functional characteristics of the nodes within the circuit (and vice versa). In other words, structural refinements of white matter tracts may precede, and even be necessary for, functional specialization of the circuit to emerge. There is also an additional possibility that developmental refinements in a downstream functional region (e.g., anterior temporal pole in the case of face processing) influence both the structural architecture of fiber tracts and the functional characteristics of neural regions that provide input/output signals into the broader circuit.

Considerations Relating to DTI Methods

One immediate question that deserves consideration is whether the pattern of findings we observed might have arisen spuriously from specific aspects of the methods we employed. For example, in using DTI, we relied on a tensor model, which cannot resolve intravoxel orientation heterogeneity (i.e., crossing fibers problem, Alexander et al. 2001; Tuch 2004). Using other diffusion imaging methods that are capable of resolving this problem (Greenberg et al. 2012) require very long scanning times (e.g., 45 min), which are especially difficult for developmental populations to withstand while being still and are unprecedented in the literature. We also used a 6-direction acquisition procedure, even though 30-direction protocols are advantageous for robust estimates of diffusivity (Jones 2004) and tractography. It is important to note that the dependence of diffusivity estimates on the sampling orientations fundamentally depends on the anisotropy in the voxels, such that the asymptotic value of the number of unique encoding directions is approximately 30 when FA values are ≥ 0.70 (Jones 2004). Critically, at lower FA values, like at the levels we detected in the ILF (range = 0.36–0.43), 6-direction protocols produce the same diffusivity estimates as do 60-direction protocols (see Jones 2004, Fig. 5).

Given these findings, it is understandable why the vast majority of developmental DTI studies, particularly those that have large samples or that are longitudinal in design, have opted to use 6-direction protocols (e.g., Klingberg et al. 2000; Schmithorst et al. 2002; Olesen et al. 2003; Baird et al. 2005; Barnea-Goraly et al. 2005; Ben Bashat et al. 2005, 2007; Snook et al. 2005, 2007; Lebel et al. 2008, 2010; Qui et al. 2008; Thomas et al. 2008; Berman et al. 2009; Kumar et al. 2009; Lebel and Christian 2009; Lebel and Beaulieu 2011; Asato et al. 2010; Barb et al. 2011), which are much shorter in duration, and therefore more tolerable for special populations, than are higher-definition DTI scans. Developmental DTI studies that use more encoding directions (e.g., Schmithorst et al. 2005; Hermoye et al. 2006; Giorgio et al. 2010; Bava et al. 2011; Clayden et al. 2012) have also not produced contrary results to the 6-direction DTI studies. This precedence to use 6-direction protocols in the majority of developmental DTI studies suggests a consensus in the field for sufficient (and possibly

optimal) developmental methods, with reduced acquisition time and sufficient sensitivity for deriving FA and diffusivity estimates. Finally, we were particularly rigorous about minimizing the concern that age-related differences in the macro- and microstructural properties of the tracts of interest are related to motion differences across the age range. To our knowledge, this is the first developmental DTI study to report age-related differences in tract properties after controlling for motion in a functional scan that occurred in the same scanning session with the DTI scan. As a result, we are confident that our findings of age-related differences in both the macro- and microstructural properties of our tracts of interest are not spuriously related to our methodological approach, even in the context of understanding these important limitations of the approach.

Conclusion

Our results suggest that there are circumscribed, disproportionately large age-related differences (and potential changes) in the ILF from childhood through early adulthood that are tightly linked with differences in the functional profile of the pre-eminent face area, the FFA, which serves a hub-like role in face perception (Nestor et al. 2011). This exciting, novel finding establishes the relationship between the structure and function in this neural circuit. This result elucidates the dynamic structural and functional changes in this network and also has implications for how development and optimization of cortical organization might occur, more generally. These findings may serve as a benchmark against which to explore perturbations in development of this system, as evident in autism, Williams syndrome, children with cataracts, and prosopagnosia (congenital or acquired in early childhood).

Funding

The research reported in this paper was supported by Pennsylvania Department of Health SAP grant 4100047862 (M.B., K.S.S.), NICHD/NIDCD P01/U19 (M.B., PI-Nancy Minshew), a post-doctoral fellowship from the National Alliance for Autism Research to Suzy Scherf and Beatriz Luna, an NSF Science of Learning Center grant, “Temporal Dynamics of Learning Center” (PI: Gary Cottrell, Co-I: M.B.), and a NSF grant (BCS0923763) to M.B.

Notes

We thank Dr Kwan-Jin Jung, Scott Kurdilla, and Debbie Viszlay from the Brain Imaging Research Center at the McGowan Center in Pittsburgh for their help in acquiring the imaging data. We are also grateful to our study families for making this research possible. *Conflict of Interest:* None declared.

References

Alexander AL, Hasan KM, Lazar M, Tsuruda JS, Parker DL. 2001. Analysis of partial volume effects in diffusion-tensor MRI. *Magn Reson Med.* 45:770–780.

Asato MR, Terwilliger R, Woo J, Luna B. 2010. White matter development in adolescence: a DTI study. *Cereb Cortex.* 20:2122–2131.

Avidan G, Hasson U, Malach R, Behrmann M. 2005. Detailed exploration of face-related processing in congenital prosopagnosia: a functional neuroimaging findings. *J Cogn Neurosci.* 17:1150–1167.

Aylward EH, Park JE, Field KM, Parsons AC, Richards TL, Cramer SC, Meltzoff AN. 2005. Brain activation during face perception: evidence of a developmental change. *J Cogn Neurosci.* 17:308–319.

Baird AA, Colvin MK, VanHorn JD, Inati S, Gazzaniga MS. 2005. Functional connectivity: integrating behavioral, diffusion tensor imaging, and functional magnetic resonance imaging data sets. *J Cogn Neurosci.* 17:687–693.

Bar M, Kassam KS, Ghuman AS, Boshyan J, Schmid AM, Dale AM, Hamalainen MS, Marinkovic K, Schacter DL, Rosen BR et al. 2006. Top-down facilitation of visual recognition. *Proc Natl Acad Sci USA.* 103:449.

Barb SM, Rodriguez-Galindo C, Wilson MW, Phillips NS, Zou P, Scoggins MA, Li Y. 2011. Functional neuroimaging to characterize visual system development in children with retinoblastoma. *Invest Ophthalmol Vis Sci.* 52:2619–2626.

Barnea-Goraly N, Menon V, Eckert M, Tamm L, Bammer R, Karchemskiy A, Dant CC, Reiss AL. 2005. White matter development during childhood and adolescence: a cross-sectional diffusion tensor imaging study. *Cereb Cortex.* 15:12:1848–1854.

Bava S, Boucquoy V, Goldenberg D, Thayer RE, Ward M, Jacobus J, Tapert SF. 2011. Sex differences in adolescent white matter architecture. *Brain Res.* 1375:41–48.

Beaulieu C. 2002. The basis of anisotropic water diffusion in the nervous system—a technical review. *NMR Biomed.* 15:7–8:435–455.

Ben Bashat D, Ben Sira L, Graif M, Pianka P, Hendler T, Cohen Y, Assaf Y. 2005. Normal white matter development from infancy to adulthood: comparing diffusion tensor and high b value diffusion weighted MR images. *J Magn Reson Imaging.* 21:5:503–511.

Ben Bashat D, Kronfeld-Duenias V, Zachor DA, Ekstein PM, Hendler T, Tarrasch R, Even A, Levy Y, Ben Sira L. 2007. Accelerated maturation of white matter in young children with autism: a high b value DWI study. *NeuroImage.* 37:1:40–47.

Benes FM, Turtle M, Khan Y, Farol P. 1994. Myelination of a key relay zone in the hippocampal formation occurs in the human brain during childhood, adolescence, and adulthood. *Arch Gen Psychiatry.* 51:6:477.

Bengtsson SL, Nagy Z, Skare S, Forsman L, Forssberg H, Ullén F. 2005. Extensive piano practicing has regionally specific effects on white matter development. *Nat Neurosci.* 8:9:1148–1150.

Berman J, Glass HC, Miller SP, Mukherjee P, Ferriero DM, Barkovich AJ, Vigneron DB, Henry RG. 2009. Quantitative fiber tracking analysis of the optic radiation correlated with visual performance in premature newborns. *Am J Neuroradiol.* 30:1:120–124.

Burgund E, Kang H, Kelly J, Buckner R, Snyder A, Petersen S, Schlaggar B. 2002. The feasibility of a common stereotactic space for children and adults in fMRI studies of development. *NeuroImage.* 17:1:184–200.

Cantlon JF, Pinel P, Dehaene S, Pelphrey KA. 2011. Cortical representations of symbols, objects, and faces are pruned back during early childhood. *Cerebr Cortex.* 21:1:191–199.

Catani M. 2007. From hodology to function. *Brain.* 130(Pt 3):602–605.

Catani M, Howard RJ, Pajevic S, Jones DK. 2002. Virtual in vivo interactive dissection of white matter fasciculi in the human brain. *NeuroImage.* 17:7:77–94.

Catani M, Jones DK, Donato R, Ffytche DH. 2003. Occipito-temporal connections in the human brain. *Brain.* 126:2093–2107.

Catani M, Thiebaut de Schotten MT. 2008. A diffusion tensor imaging tractography atlas for virtual in vivo dissections. *Cortex.* 44:8:1105–1132.

Cercignania M, Bozzalia M, Iannuccia G, Comib G, Filippia M. 2001. Magnetisation transfer ratio and mean diffusivity of normal appearing white and grey matter from patients with multiple sclerosis. *J Neurol Neurosurg Psychiatry.* 70:3:311–317.

Clayden JD, Jentschke S, Muñoz M, Cooper JM, Chadwick MJ, Banks T, Vargha-Khadem F. 2012. Normative development of white matter tracts: similarities and differences in relation to age, gender, and intelligence. *Cerebr Cortex.* 22:8:1738–1747.

Cohen Kadosh K, Cohen Kadosh R, Dick F, Johnson MH. 2011. Developmental changes in effective connectivity in the emerging core face network. *Cerebr Cortex.* 21:1389–1394.

Crosby EC, Humphrey T, Lauer EW. 1962. Correlative anatomy of the nervous system. New York: Macmillan.

Demerens C, Stankoff B, Logak M, Anglade P, Allinquant B, Couraud F, Zalc B, Lubetzki C. 1996. Induction of myelination in the central nervous system by electrical activity. *Proc Natl Acad Sci.* 93:18:9887.

- Durston S, Davidson MC, Tottenham N, Galvan A, Spicer J, Fossella JA, Casey BJ. 2006. A shift from diffuse to focal cortical activity with development. *Develop Sci*. 9:11–20.
- Fairhall S, Ishai A. 2007. Effective connectivity within the distributed cortical network for face perception. *Cereb Cortex*. 17:10:2400–2406.
- Fox CJ, Iaria G, Barton JJ. 2008. Disconnection in prosopagnosia and face processing. *Cortex*. 44:8:996–1009.
- Gathers AD, Bhatt R, Corbly CR, Farley AB, Joseph JE. 2004. Developmental shifts in cortical loci for face and object recognition. *Neuroreport*. 15:10:1549–1553.
- Gauthier I, Tarr MJ, Moylan J, Skudlarski P, Gore JC, Anderson AW. 2000. The fusiform “face area” is part of a network that processes faces at the individual level. *J Cogn Neurosci*. 12:3:495–504.
- Genovese CR, Lazar NA, Nichols T. 2002. Thresholding of statistical maps in functional neuroimaging using the false discovery rate. *NeuroImage*. 15:4:870–878.
- Giorgio A, Watkins KE, Chadwick M, James S, Winmill L, Douaud G, De Stefano N, Matthews PM, Smith SM, Johansen-Berg H et al. 2010. Longitudinal changes in grey and white matter during adolescence. *NeuroImage*. 49:1:94–103.
- Gloor P. 1997. *The temporal lobe and the limbic system*. New York: Oxford University Press.
- Gobbini M, Haxby JV. 2007. Neural systems for recognition of familiar faces. *Neuropsychologia*. 45:1:32–41.
- Gogtay N, Giedd JN, Lusk L, Hayashi KM, Greenstein D, Vaituzis C, Nugent TF III, Herman DH, Clasen LS, Toga AW et al. 2004. Dynamic mapping of human cortical development during childhood through early adulthood. *Proc Natl Acad Sci USA*. 101:21:8174–8179.
- Golarai G, Ghahremani DG, Whitfield-Gabrieli S, Reis A, Eberhardt JL, Gabrieli JD, Grill-Spector K. 2007. Differential development of high-level visual cortex correlates with category-specific recognition memory. *Nat Neurosci*. 10:4:512–522.
- Golarai G, Liberman A, Yoon JM, Grill-Spector K. 2010. Differential development of the ventral visual cortex extends through adolescence. *Front Hum Neurosci*. 3:80.
- Greenberg AS, Verstynen T, Chiu YC, Yantis S, Schneider W, Behrmann M. 2012. Visuotopic cortical connectivity underlying attention revealed with white-matter tractography. *J Neurosci*. 32:8:2773–2782.
- Gschwind M, Pourtois G, Schwartz S, Van De Ville D, Vuilleumier P. 2012. White-matter connectivity between face-responsive regions in the human brain. *Cereb Cortex*. 22:15:1564–1576.
- Gyllenstein L, Malmfors T. 1963. Myelination of the optic nerve and its dependence on visual function: a quantitative investigation in mice. *J Embryol Exp Morphol*. 11:1:255–266.
- Hasson U, Nir Y, Levy I, Fuhrmann G, Malach R. 2004. Intersubject synchronization of cortical activity during natural vision. *Science*. 303:16:1634–1640.
- Haxby JV, Hoffman EA, Gobbini MI. 2002. Human neural systems for face recognition and social communication. *Biol Psychiatry*. 51:1:59–67.
- Haxby JV, Petit L, Ungerleider LG, Courtney SM. 2000. Distinguishing the functional roles of multiple regions in distributed neural systems for visual working memory. *NeuroImage*. 11:5:380–391.
- Hermoye L, Saint-Martin C, Cosnard G, Lee SK, Kim J, Nassogne MC, Menten R, Claputy P, Donohue PK, Hua K et al. 2006. Pediatric diffusion tensor imaging: normal database and observation of the white matter maturation in early childhood. *NeuroImage*. 29:2:493–504.
- Hoffman EA, Haxby JV. 2000. Distinct representations of eye gaze and identity in the distributed human neural system for face perception. *Nat Neurosci*. 3:3:80–84.
- Humphreys K, Hasson U, Avidan G, Minshew N, Behrmann M. 2008. Cortical patterns of category-selective activation for faces, places and objects in adults with autism. *Autism Res*. 1:52–63.
- Ishai A. 2008. Let's face it: It's a cortical network. *NeuroImage*. 40:2:415–419.
- Jiang H, van Zijl PC, Kim J, Pearlson GD, Mori S. 2006. DtiStudio: resource program for diffusion tensor computation and fiber bundle tracking comput methods programs. *Comput Methods Programs Biomed*. 81:2:106–116.
- Jones DK. 2004. The effect of gradient sampling schemes on measures derived from diffusion tensor MRI: a monte carlo study. *Magn Reson Med*. 51:4:807–815.
- Jones DK, Symms MR, Cercignani M, Howard RJ. 2005. The effect of filter size on VBM analyses of DT-MRI data. *Neuroimage*. 26:5:546–554.
- Joseph JE, Gathers AD, Bhatt RS. 2011. Progressive and regressive developmental changes in neural substrates for face processing: testing specific predictions of the interactive specialization account. *Develop Sci*. 14:2:227–241.
- Kanwisher N, McDermott J, Chun MM. 1997. The fusiform face area: a module in human extrastriate cortex specialized for face perception. *J Neurosci*. 17:11:4302–4311.
- Klingberg T, Hedehus M, Temple E, Salz T, Gabrieli JD, Moseley ME, Poldrack RA. 2000. Microstructure of temporo-parietal white matter as a basis for reading ability: evidence from diffusion tensor magnetic resonance imaging. *Neuron*. 25:2:493–500.
- Kumar A, Juhasz C, Asano E, Sundaram SK, Makki MI, Chugani DC, Chugani HT. 2009. Diffusion tensor imaging study of the cortical origin and course of the corticospinal tract in healthy children. *Am J Neuroradiol*. 30:10:1963–1970.
- Lebel C, Beaulieu C. 2011. Longitudinal development of human brain wiring continues from childhood into adulthood. *J Neurosci*. 31:30:10937–10947.
- Lebel C, Christian B. 2009. Lateralization of the Arcuate Fasciculus from childhood to adulthood and its relation to cognitive abilities in children. *Hum Brain Mapp*. 30:35:3563–3573.
- Lebel C, Walker L, Leemans A, Phillips L, Beaulieu C. 2008. Microstructural maturation of the human brain from childhood to adulthood. *NeuroImage*. 40:3:1044–1055.
- Lebel C, Caverhill-Godkewitsch S, Beaulieu C. 2010. Age-related regional variations of the corpus callosum identified by diffusion tensor tractography. *NeuroImage*. 52:1:20–31.
- Loenneker T, Klaver P, Bucher K, Lichtensteiger J, Imfeld A, Martin E. 2011. Microstructural development: organizational differences of the fiber architecture between children and adults in dorsal and ventral visual streams. *Hum Brain Mapp*. 32:6:935–946.
- Lori NF, Akbudak E, Shimony JS, Cull TS, Snyder AZ, Guillery RK. 2002. Diffusion tensor fiber tracking of human brain connectivity: acquisition methods, reliability analysis and biological results. *NMR Biomed*. 15:4:494–515.
- Lövdén M, Bodammer NC, Kühn S, Kaufmann J, Schütze H, Tempelmann C, Heinze HJ, Duzel E, Schmiedek F, Lindenberger U. 2010. Experience-dependent plasticity of white-matter microstructure extends into old age. *Neuropsychologia*. 48:13:3878–3883.
- McIntosh AR. 2004. Contexts and catalysts: a resolution of the localization and integration of function in the brain. *Neuroinformatics*. 2:2:175–182.
- Mesulam MM. 1990. Large-scale neurocognitive networks and distributed processing for attention, language, and memory. *Ann Neurol*. 28:5:597–613.
- Mori S, Crain BJ, Chacko VP, van Zijl PC. 1999. Three-dimensional tracking of axonal projections in the brain by magnetic resonance imaging. *Ann Neurol*. 45:2:265–269.
- Nemani AK, Atkinson IC, Thulborn KR. 2009. Investigating the consistency of brain activation using individual trial analysis of high-resolution fmri in the human primary visual cortex. *NeuroImage*. 47:14:1417–1424.
- Nestor A, Plaut DC, Behrmann M. 2011. Unraveling the distributed neural code of facial identity through spatiotemporal pattern analysis. *Proc Natl Acad Sci USA*. 108:24:9998–10003.
- Olesen PJ, Nagy Z, Westerberg H, Klingberg T. 2003. Combined analysis of DTI and fMRI data reveals a joint maturation of white and grey matter in a fronto-parietal network. *Brain Res Cogn Brain Res*. 18:1:48–57.
- Passarotti AM, Paul BM, Bussiere JR, Buxton RB, Wong EC, Stiles J. 2003. The development of face and location processing: an fMRI study. *Develop Sci*. 6:1:100–117.

- Passarotti AM, Smith J, DeLano M, Huang J. 2007. Developmental differences in the neural bases of the face inversion effect show progressive tuning of face-selective regions to the upright orientation. *NeuroImage*. 34:1708–1722.
- Peelen MV, Glaser B, Vuilleumier P, Eliez S. 2009. Differential development of selectivity for faces and bodies in the fusiform gyrus. *Developmental Science*. 12:116–125.
- Pelphrey KA, Lopez J, Morris JP. 2009. Developmental continuity and change in responses to social and nonsocial categories in human extrastriate visual cortex. *Front Hum Neurosci*. 3:25.
- Philippi CL, Mehta S, Grabowski T, Adolphs R, Rudrauf D. 2009. Damage to association fiber tracts impairs recognition of the facial expression of emotion. *J Neurosci*. 29:15089–15099.
- Qiu D, Tan LH, Zhou K, Khong PL. 2008. Diffusion tensor imaging of normal white matter maturation from late childhood to young adulthood: voxel-wise evaluation of mean diffusivity, fractional anisotropy, radial and axial diffusivities, and correlation with reading development. *NeuroImage*. 41:223–232.
- Rudrauf D, David O, Lachaux JP, Kovach CK, Martinerie J, Renault B, Damasio A. 2008. Rapid interactions between the ventral visual stream and emotion-related structures rely on a two-pathway architecture. *J Neurosci*. 28:2793–2803.
- Saygin ZM, Osher DE, Koldewyn K, Reynolds G, Gabrieli JD, Saxe RR. 2011. Anatomical connectivity patterns predict face selectivity in the fusiform gyrus. *Nat Neurosci*. 15:321–327.
- Scherf K, Behrmann M, Humphreys K, Luna B. 2007. Visual category-selectivity for faces, places and objects emerges along different developmental trajectories. *Developmental Science*. 10:115–130.
- Scherf K, Luna B, Minshew N, Behrmann M. 2010. Location, location: alterations in the functional topography of face- but not object- or place-related cortex in adolescents with autism. *Front Hum Neurosci*. 4:1–5.
- Scherf KS, Luna B, Avidan G, Behrmann M. 2011. “What” precedes “which”: developmental neural tuning in face- and place-related cortex. *Cerebr Cortex*. 9:1963–1980.
- Schlegel AA, Rudelson JJ, Tse PU. 2012. White matter structure changes as adults learn a second language. *J Cogn Neurosci*. 24:1664–1670.
- Schmahmann JD, Pandya DN, Wang R, Dai G, D’Arceuil HE, de Crespigny AJ, Wedeen VJ. 2007. Association fibre pathways of the brain: parallel observations from diffusion spectrum imaging and autoradiography. *Brain*. 130(Pt 3):630–653.
- Schmithorst VJ, Wilke M, Dardzinski BJ, Holland SK. 2005. Cognitive functions correlate with white matter architecture in a normal pediatric population: a diffusion tensor MRI study. *Hum Brain Mapp*. 26:139–147.
- Schmithorst VJ, Wilke M, Dardzinski BJ, Holland SK. 2002. Correlation of white matter diffusivity and anisotropy with age during childhood and adolescence: a cross-sectional diffusion-tensor MR imaging study. *Radiology*. 222:212–218.
- Snook L, Paulson LA, Roy D, Phillips L, Beaulieu C. 2005. Diffusion tensor imaging of neurodevelopment in children and young adults. *NeuroImage*. 26:1164–1173.
- Snook L, Plewes C, Beaulieu C. 2007. Voxel based versus region of interest analysis in diffusion tensor imaging of neurodevelopment. *NeuroImage*. 34:243–252.
- Song SK, Yoshino J, Le TQ, Lin SJ, Sun SW, Cross AH, Armstrong RC. 2005. Demyelination increases radial diffusivity in corpus callosum of mouse brain. *NeuroImage*. 26:132–140.
- Supekar K, Uddin LQ, Prater K, Amin H, Greicius MD, Menon V. 2010. Development of functional and structural connectivity within the default mode network in young children. *NeuroImage*. 52:290–301.
- Thiebaut de Schotten M, Ffytche DH, Bizzi A, Dell’Acqua F, Allin M, Walshe M, Murray R, Williams SC, Murphy DGM, Catani M. 2011. Atlas location, asymmetry and inter-subject variability of white matter tracts in the human brain with MR diffusion tractography. *NeuroImage*. 54:49–59.
- Thomas C, Avidan G, Humphreys K, Jung KJ, Gao F, Behrmann M. 2009. Reduced structural connectivity in ventral visual cortex in congenital prosopagnosia. *Nat Neurosci*. 12:29–31.
- Thomas C, Baker CI. 2012. Teaching an adult brain new tricks: a critical review of evidence for training-dependent structural plasticity in humans. *NeuroImage*. 73:225–236.
- Thomas C, Humphreys K, Jung KJ, Minshew N, Behrmann M. 2011. The anatomy of the callosal and visual-association pathways in high-functioning autism: a DTI tractography study. *Cortex*. 47:863–873.
- Thomas C, Moya L, Avidan G, Humphreys K, Jung K, Peterson M, Behrmann M. 2008. Reduction in white matter connectivity, revealed by diffusion tensor imaging, may account for age-related changes in face perception. *J Cogn Neurosci*. 20:268–284.
- Tuch DS. 2004. Q-ball imaging. *Magn Reson Med*. 52:1358–1372.
- Uddin LQ, Supekar KS, Ryali S, Menon V. 2011. Dynamic reconfiguration of structural and functional connectivity across core neurocognitive brain networks with development. *J Neurosci*. 31:18578–18589.
- Vuilleumier P, Pourtois G. 2007. Distributed and interactive brain mechanisms during emotion face perception: evidence from functional neuroimaging. *Neuropsychologia*. 45:174–194.
- Wakana S, Caprihan A, Panzenboeck MM, Fallon JH, Perry M, Gollub RL, Hua K, Zhang J, Jiang H, Dubey P et al. 2007. Reproducibility of quantitative tractography methods applied to cerebral white matter. *NeuroImage*. 36:630–644.
- Westin CF, Maier SE, Mamata H, Nabavi A, Jolesz FA, Kikinis R. 2002. Processing and visualization for diffusion tensor. *MRI Med Image Anal*. 6:93–108.
- Wilke M, Lidzba K, Staudt M, Buchenau K, Grodd W, Krägeloh-Mann I. 2005. Comprehensive language mapping in children, using functional magnetic resonance imaging: What’s missing counts. *Neuroreport*. 16:915–919.
- Xue R, van Zijl PCM, Crain BJ, Solaiyappan M, Mori S. 1999. In vivo three-dimensional reconstruction of rat brain axonal projections by diffusion tensor imaging. *Magn Reson Med*. 42:1123–1127.
- Yakovlev PI, Lecours AR. 1967. The myelogenetic cycles of regional maturation of the brain. In Minkowski A, editors. *Regional development of the brain in early life*. Oxford: Blackwell Scientific. p. 3–70.
- Yovel G, Tambini A, Brandman T. 2008. The asymmetry of the fusiform face area is a stable individual characteristic that underlies the left-visual-field superiority for faces. *Neuropsychologia*. 46:3061–3068.